FINITE ELEMENT BASED STABILITY-CONSTRAINED WEIGHT MINIMIZATION OF SANDWICH COMPOSITE DUCTS FOR AIRSHIP APPLICATIONS

by

URMI B. KHODE

Presented to the Faculty of the Graduate School of

The University of Texas at Arlington in Partial Fulfillment

of the Requirements

for the Degree of

MASTER OF SCIENCE IN AEROSPACE ENGINEERING

THE UNIVERSITY OF TEXAS AT ARLINGTON

August 2011

ACKNOWLEDGEMENTS

I would like to express my deepest gratitude and appreciation to my advisor Dr. D. Stefan Dancila, for believing in me and my capabilities. His invaluable supervision, guidance and unflinching encouragement have made this research possible. His ever-encouraging quote “Make me proud”, after assigning me a task, always pumped up my zest to work in his guided direction. I am very thankful to Dr. Dancila for giving me a lifetime quote, as it will help me excel in my future endeavors.

Secondly, I would like to thank Dr. Kent Lawrence for his invaluable technical suggestions in the area of FEM that helped me in my thesis. I am also thankful to Dr. Armanios and Dr. Chan for serving on my thesis committee.

A special thanks to Bhumil Diwanji for his constant friendly advice throughout my curriculum and also to my family here in Arlington, consisting of my friends and roommates, for always making me feel at home and encouraging, cheering and believing in me when I ceased to do so. I would also like to thank my lab mates Shailesh Divey, Julie Cline, Sthanu Mahadev, Michael Tadros, and Daniel Mockler and the postdoctoral fellows Dr. Jennifer Goss, Dr. Robert Haynes, and Dr. Xinyuan Tan for their assistance and technical support. It was fun and beneficial studying and working together. I would like to especially thank Dr. Robert Haynes for his constant guidance and continuous support.

Above all, with all due respect I profoundly acknowledge my parents Bharat Khode and Vandana Khode and my brother Kshitij Khode for their love, support and motivation that helped me accomplish my goals. With all my love to my grandfather, the late Krishnakant Khode, who wanted to see me graduate. I dedicate this thesis to him.

July 14, 2011

ABSTRACT

FINITE ELEMENT BASED STABILITY-CONSTRAINED WEIGHT MINIMIZATION OF SANDWICH COMPOSITE DUCTS FOR AIRSHIP APPLICATIONS

Urmi B. Khode, M.S.

The University of Texas at Arlington, 2011

Supervising Professor: D. Stefan Dancila

High Altitude Long Endurance (HALE) airships are platform of interest due to their persistent observation and persistent communication capabilities. A novel HALE airship design configuration incorporates a composite sandwich propulsive hull duct between the front and the back of the hull for significant drag reduction via blown wake effects. The sandwich composite shell duct is subjected to hull pressure on its outer walls and flow suction on its inner walls which result in in-plane wall compressive stress, which may cause duct buckling. An approach based upon finite element stability analysis combined with a ply layup and foam thickness determination weight minimization search algorithm is utilized. Its goal is to achieve an optimized solution for the configuration of the sandwich composite as a solution to a constrained minimum weight design problem, for which the shell duct remains stable with a prescribed margin of safety under prescribed loading. The stability analysis methodology is first verified by comparing published analytical results for a number of simple cylindrical shell configurations with FEM counterpart solutions obtained using the commercially available code ABAQUS. Results show that the approach is effective in identifying minimum weight composite duct

configurations for a number of representative combinations of duct geometry, composite material and foam properties, and propulsive duct applied pressure loading.

TABLE OF CONTENTS

LIST OF ILLUSTRATIONS

LIST OF TABLES

NOMENCLATURE

A_p	Area swept by the propeller blades
C_d	Drag coefficient =0.12
D	Flexural stiffness
$D_{airship}$	Drag on airship
E	Young's modulus
L	Length of the cylinder
P	Pressure
P_∞	Pressure at far field
P_1	Pressure at inlet of the duct
P_2	Pressure immediately ahead of the propeller disc
P_3	Pressure immediately behind the propeller disc
P_4	Pressure at the exit of the duct
P_{part1}	Pressure distribution on the front part of the duct
P_{part2}	Pressure distribution on the rear part of the duct
R	Radius of the airship
T	Thrust
V_∞	Free-stream velocity
V_1	Velocity of air at inlet of the duct
V_2	Velocity of air immediately ahead of the propeller disc
V_3	Velocity of air immediately behind the propeller disc
V_4	Velocity of air at the exit of the duct
V_i	Induced velocity at propeller disc

V_p	Velocity of air at the propeller disc
Z	Batdorf's parameter
k_y	Critical circumferential stress coefficient
$P_{buckling}$	Buckling pressure
r	Radius of the cylinder or duct
t	Thickness of the cylinder
t_f	Thickness of foam
Δp	Pressure jump across the propeller disc
σ_y	Circumferential stress
ρ	Density
ν	Poisson's ratio

CHAPTER 1

INTRODUCTION

1.1 Background

1.1.1 High Altitude Long Endurance (HALE) Airships

The airship is the oldest vehicle used for controlled flight aerial operations. The first flight ever to be carried out by man was on November 21st, 1783 in a hot air balloon made by the Montgolfier brothers, Joseph–Michel and Jacques–Etienne [1]. They invented the Montgolfier-style hot air balloon, a spindle shaped globe aérostatique, made of fabric and paper gores. Hot air balloons are lighter-than-air vehicles that use buoyancy, which is dependent on the difference in density between the surrounding displaced volume of air and the fluid enclosed in the hull. The airship works on the same principle of buoyancy for generating most or all of the necessary lift, without energy expense, unlike aircraft, which spend energy to remain in motion in order to develop dynamic lift. In recent years the need for persistent observation capabilities and carrying heavy loads over longer period of time with very low fuel consumption has renewed the interest in these vehicles as a possible long-endurance aerial platform.

High Altitude Long Endurance (HALE) airships are platforms of interest for observation and line-of-sight communications due to their persistent flight capabilities. HALE airships have gained attention due to their potential to improve communications through wide area line-of-sight ground coverage available from high altitude station locations. A single aerial platform can cover an area of 250-300 nm radius from an altitude of 65 kft, potentially replacing a large number of terrestrial communication antenna towers. HALE airships can operate autonomously in the stratosphere for ultra-long endurance, sustained missions, providing real-time Intelligence Surveillance and Reconnaissance (ISR), line-of-sight communications between ground stations and airships, and relayed ground-airship-ground communications. For broadcasting and communication systems, HALE airships are better candidates as compared to satellites due to their lower development, maintenance, and operational cost.

1.1.2 HALE Airship Configuration of Interest

Hull drag is proportional to the square of airspeed and the required propulsion power is proportional to the third power of airspeed; therefore, it is essential to minimize the aerodynamic drag to maximize the propulsion efficiency for effective station-keeping performance of an airship. A small reduction in the hull drag can result in significant fuel saving, which in turn leads to greater payload capacity and an increased endurance.

Experimental investigations were conducted on smooth solid spheres having front-to-back ducts by Suryanarayana *et al* [2] to study the drag reduction by passive ventilation. A significant drag reduction for high *Re* number was observed.

A novel unconventional HALE airship design has a toroidal configuration, with a hull duct connecting the front and the back. The passive and/or propulsive duct flow significantly reduces hull drag via blowing of the wake region. This enables the use of less elongated, lower aspect ratio hulls - in the limit spherical - which reduce the envelope mass and airship pitch and yaw moments of inertia for a given hull volume.

The hull duct wall is subject to hull overpressure on its outer surface and duct-flow-induced dynamic pressures on its inner surface; therefore, a structure capable of resisting compressive loads is necessary to keep the duct open. The duct structure will develop in-plane wall compressive loading, resulting in potential loss of stability. Due to the need to minimize weight, composite sandwich configurations are lead candidates for hull duct structures.

1.2 Research Objectives

In this work a weight minimization investigation for composite sandwich ducts subject to stability constraints under applied lateral pressure is undertaken using a finite element approach. The duct configurations and pressure loading investigated are associated with their use in a novel toroidal, ducted hull airship design which is using the passive and propulsive flow through the duct for significant drag reduction. The sandwich composite shell duct experiences hull overpressure on its outer lateral surface and flow suction on its interior, resulting in in-plane compressive stresses, which may cause loss of stability. The finite element stability analysis methodology is first verified by comparing published analytical results for a number of simple homogeneous isotropic cylindrical shell configurations with the FEM counterpart solutions obtained by using the commercially available code ABAQUS. The finite element based stability analysis combined with a stand alone ply search algorithm are subsequently utilized to achieve an optimal configuration of the sandwich composite duct as a solution to minimum weight design problem for which the shell duct remains stable, with an imposed margin of safety, under the applied loading.

1.3 Roadmap

A literature survey on buckling of thin circular cylinderical shells is conducted and summarized in Chapter 2, followed by Chapter 3, which covers the verification study of FEM-based stability analysis, involving comparison of FEM counterpart solutions obtained using ABAQUS to published analytical results available in the literature. In Chapter 4, a FEM-based optimization methodology is developed to find the optimal feasible configuration for the sandwich composite duct as a solution to minimum weight design problem. The results and discussions are reported in Chapter 5, followed in Chapter 6 by conclusions and recommendations.

CHAPTER 2

LITERATURE SURVEY

Prior research into stability of thin metal shells under various loading and end conditions has been conducted, as they are widely used in aircraft, rockets, submarines, cooling towers, nuclear reactors, etc. Batdorf [3] derived the buckling stresses for simply supported circular cylinders loaded with axial pressure, lateral pressure, and hydrostatic pressure by expressing them in terms of two non-dimensional parameters: one dependent on the circumferential stress and the other dependent on the geometry of the cylinder. For a specific case of cylinder subjected to lateral pressure, the critical circumferential stress coefficient, k_y, is given by

$$k_y = 1.04Z^{1/2} \qquad 100 < Z < 5\left(\frac{r}{t}\right)^2\left(1-\nu^2\right) \tag{2.1}$$

where the Batdorf's parameter, Z, is

$$Z = \frac{L^2}{rt}\sqrt{1-\nu^2} \tag{2.2}$$

r, t, and L are the radius, thickness, and length of the cylinder, respectively, and ν is Poisson's ratio. The flexural stiffness, D, the circumferential stress, σ_y , and the buckling pressure, $p_{buckling}$, are

$$D = \frac{Et^3}{12(1-\nu^2)} \tag{2.3}$$

$$\sigma_y = k_y \frac{\pi^2 D}{L^2 t} \tag{2.4}$$

$$p_{buckling} = \sigma_y \frac{t}{r} \tag{2.5}$$

Equation (2.1) was utilized to perform the verification study of FEM-based stability analysis.

Sandwich structures are known for being weight-efficient and find extensive application in the aerospace industry. The sandwich structure is made of high-stiffness fiber-reinforced composite as face sheets and low-density foam as core material. The advantage of composite sandwich structures is that they offer high stiffness and high buckling load capacity than homogeneous materials [4]. Adali *et al* [5] conducted a weight optimization study on composite laminates of graphite-only, glass fiber-only, and hybrid laminates of graphite and glass fiber to determine the optimal stacking sequence that withstands the maximum buckling load using discrete sets of 0˚, ±45˚ and 90˚ ply orientations under uniaxial and biaxial loading on plates with various aspect ratios. It was observed that in both the loading cases a significant weight reduction was seen, when hybrid laminates of half graphite and half glass fiber were used as compared to one material system only. Optimization studies to find minimum mass were performed to determine the best material combination and stacking sequence for composite sandwich cylindrical shells subject to buckling under axial load [6,7]. Xie *et al* [8] described a method for analyzing the maximum buckling strength of cylinder shell made of hybrid-fiber multilayer-sandwich under external pressure for optimum fiber orientation angle and weigh factor.

All of the studies mentioned above consisted of two stages: first, several subsets of face sheet thicknesses, the core thicknesses, and the face sheet fiber orientation angles were optimized, for a design buckling load capacity and cost constraints, and second, the configuration with least mass was selected. A case study [9] on finding an optimum design for buckling and overstressed fiber-reinforced composite cylindrical skirts for rocket cases was studied for a better understanding of optimization procedures concerning buckling of composites. In this work, a minimum mass optimization procedure for a composite-sandwich convergent propulsive duct for an airship subjected to stability constraints was carried out using an FEM-based iterative method for a defined set of fiber orientation angles for optimal composite sandwich solutions.

CHAPTER 3

VERIFICATION OF FEM-BASED STABILITY ANALYSIS

Circular thin-shell cylinders with the material properties of steel and different values of *Z*, were solved for their buckling load in this study to verify the FEM-based approach. The analytical solutions for buckling of simply supported circular cylinders subjected to lateral pressure were compared with ABAQUS FEM results for various geometric configurations. The material properties used in the analysis were E=210.0 GPa and ν=0.3.

3.1 Model Geometric Specifications

Six different circular cylindrical configurations were considered in this verification study, which are presented in Table 3.1.

Table 3.1 Cylinder configurations for FEM analysis

	Batdorf's Parameter (*Z*)	Length	Radius	Thickness
Case 1	238.458	5	2	0.05
Case 2	4208.46	3	1	0.00204
Case 3	5728.31	3.5	1	0.00204
Case 4	11690.4	5	1	0.00204
Case 5	22913.2	7	1	0.00204
Case 6	46761.7	10	1	0.00204

3.2 Applied Loads and Boundary Conditions

The edges of the cylinders were simply supported and were defined in ABAQUS in a cylindrical coordinate system. To avoid rigid body motion, a node was fixed in the axial direction at one of the edges. For a uniform buckling factor of 1 applied on the outer walls of the cylinder, ABAQUS returned the buckling pressure. Figure 3.1 represents the simply supported boundary conditions.

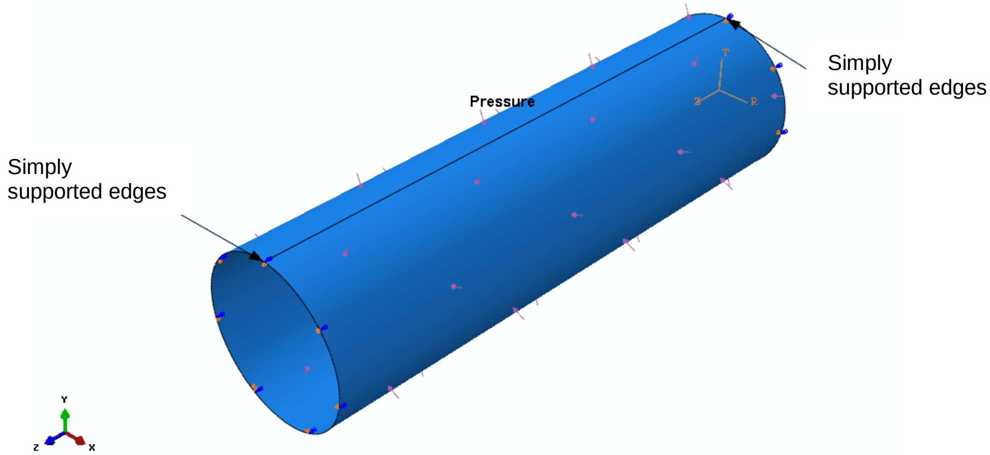

Figure 3.1 Simply supported boundary conditions

3.3 Mesh Refinement Solution Convergence Study

The 8-node reduced-integration S8R5 cubic doubly curved thin-shell element was used to model the structure. A mesh refinement study was performed for the first buckling mode until the solution converged to a percentage residue of less than 0.05%. A sample convergence plot and the mesh for the Case 5, where *Z*=22913.2 is shown in Figures 3.2 and 3.3, respectively.

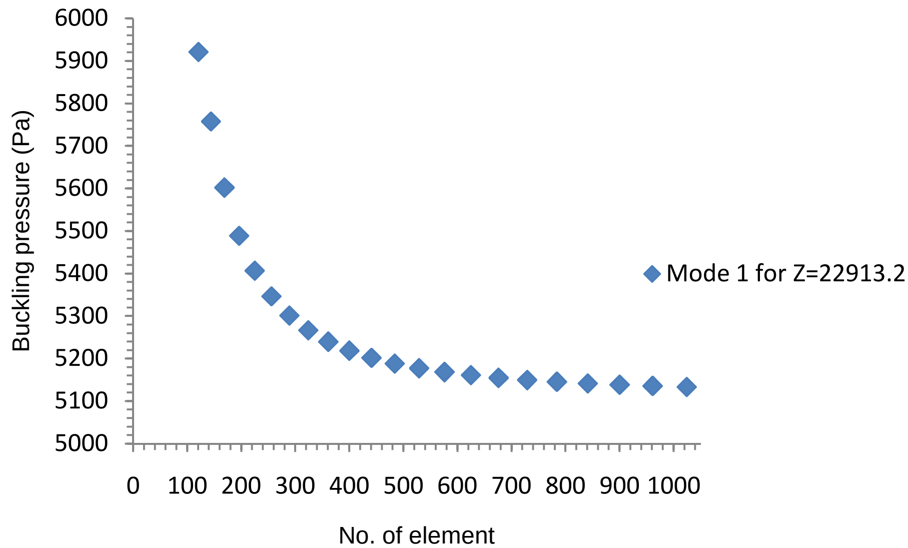

Figure 3.2 Mesh refinement solution convergence plot for mode 1 for Z=22913.2

For this case the minimum mesh required for the solution to converge at percentage residue less than 0.05% was 1024 elements.

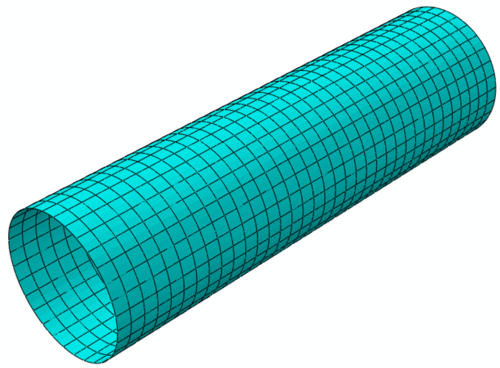

Figure 3.3 Mesh of 1024 elements for Case 5, Z=22913.2

3.4 Results and Discussions

Figure 3.4 plots the analytical solution Eq. (2.1) and ABAQUS results.

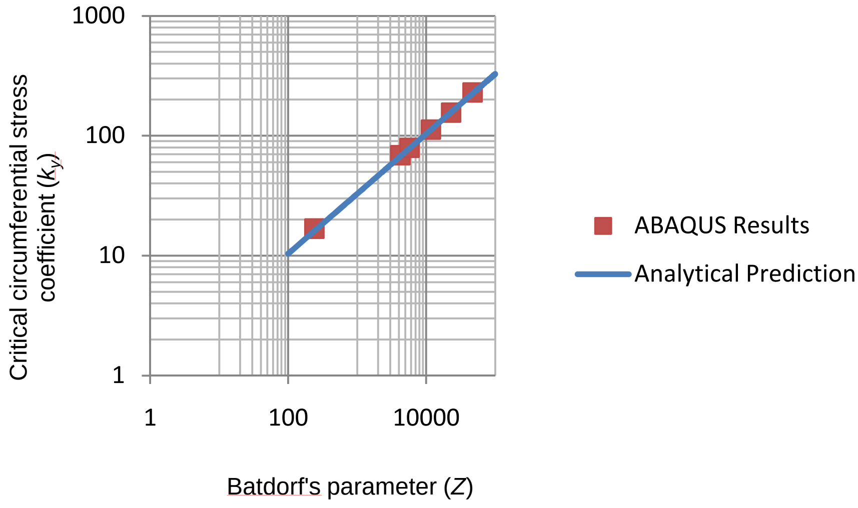

Figure 3.4 Comparison of analytical and FEM results for simply supported homogeneous isotropic cylinders

ABAQUS results are in the form of buckling pressure; hence to determine the critical circumferential stress coefficient that corresponds to this pressure, Equations 2.1 to 2.5 were used. The results converged to a within 2.28% error of the analytical solution. By comparing the FEM results and the analytical solutions, it was concluded that the method to solve for buckling of shells in the FEM code was accurate.

CHAPTER 4

MINIMUM WEIGHT STRUCTURAL OPTIMIZATION

4.1 FEM-Based Stability Analysis

Optimization is the process of finding the best solution from a feasible set of solutions that minimizes the desired objective function. The purpose of this chapter is to develop a methodology to optimize for minimum weight of a structural component, such as shell ducts, subjected to stability constraints with regard to a specified margin of safety of 50%. A representative model was considered to exemplify the FEM-based methodology.

4.1.1 Model Geometric Specification

For the results published by Suryanarayana *et al* [2], for significant drag reduction over spherical shaped bodies, the radius of the duct has 15% the radius of the spherical body. The airship model considered in this study has a radius of 20 m; hence, the duct radius at the propeller was calculated to be 3 m. To improve the performance of the propulsive duct a convergent duct design was proposed. The dimensions of the representative model are presented in Table 4.1. The front and the side view of the hull duct assembly are shown in Figure 4.1 and Figure 4.2, respectively.

Table 4.1 Geometric dimensions of representative model

Geometric Feature	**Dimensions**
Radius of airship	20 m
Radius of the duct at inlet	4.24 m
Radius at the duct at propeller	3 m
Radius of the duct at exit	2.12 m

Figure 4.1 Front view of the airship with propulsive duct

Figure 4.2 Side view of the airship with propulsive duct

The convergent duct was modeled in ABAQUS by using a set of geometric construction points derived from the prescribed set of dimensions given in Table 4.1 to form a polynomial function,

$$r(y) = 0.000454951y^2 - 0.0712311y + 4.24264 \tag{4.1}$$

where y is the axial dimension along the convergent duct from 0 m to 40 m and r is the radius of the duct.

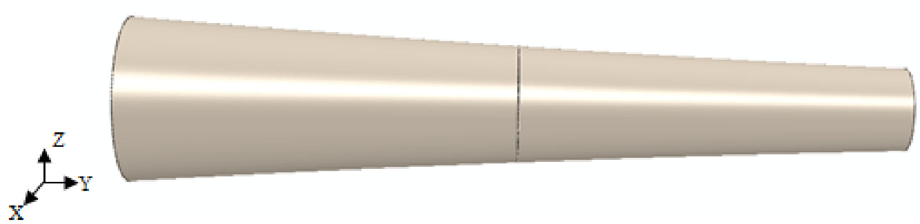

Figure 4.3 Geometry of the convergent duct

The convergent duct was modeled in two parts: the front part and the rear part, and the pressure distribution were defined along the length of the duct which is explained in detail in section 4.1.4. To make the model a continuum, tie constraints on nodes of aligned edges were imposed in the interaction module of ABAQUS. A tie constraint joins the two separate edges together so that there is no relative motion between them. This type of constraints allows two regions to fuse together even though the meshes created on the surface of the region are dissimilar. One can define tie constraints between edges of the wire or between faces of solid or shell [10]. A verification study was performed to analyze the discrepancies in the solutions of tie constrained model and uniform geometrical model for buckling analysis. A circular steel cylinder made of multiple sections was fused together by tie constraints. The cylinder was pinned at edges and subjected to uniform pressure. The results of this model were compared to a pinned edge, steel circular cylinder made of uniform section subjected to a uniform constant pressure. The study concluded that the results for both the FEM model converged with difference of 0.0% for the first three buckling mode pressure and mode shape.

4.1.2 Material Properties

The sandwich composite was made of a graphite/epoxy [11] face sheet material having ply thickness of 125μm and H100 divinycell foam [12] as core material. The material properties of the graphite/epoxy and foam are given in Tables 4.2 and Table 4.3, respectively.

Table 4.2 Graphite/Epoxy face sheet material properties

E_{11}	155.0 GPa
E_{22}	12.10 GPa
E_{33}	12.10 GPa
ν_{23}	0.458
ν_{13}	0.248
ν_{12}	0.248
G_{23}	4.15 GPa
G_{13}	4.40 GPa
G_{12}	4.40 GPa
ρ	1590 kg/m^3

Table 4.3 Foam core material properties

E	111.0 MPa
ν	0.1
ρ	100 kg/m^3

4.1.3 Operating Conditions

The optimization of the sandwich composite was undertaken in this research for the airship operating at three different altitudes. In the first case the composite sandwich duct was optimized for the airship operating at sea level; in the second case the composite sandwich duct was optimized for an airship operating at the height of 32.5 kft (10 km) where the strongest winds are expected and lastly at the height of 65 kft (20 km) above sea level. For these operating levels the atmospheric properties like pressure, density and wind velocity were known and are given in Tables 4.4, 4.5, and 4.6.

Table 4.4 Standard atmospheric properties at Earth's surface (altitude at Sea Level)

Atmospheric Parameter	**Value**
Pressure	101,325 Pa
Density	1.225 kg/m^3
Velocity profile at altitude	20 m/s

Table 4.5 Standard atmospheric properties at altitude 32.5 kft

Atmospheric Parameter	**Value**
Pressure	26,677.2 Pa
Density	0.415 kg/m^3
Velocity profile at altitude	55 m/s

Table 4.6 Standard atmospheric properties at altitude 65 kft

Atmospheric Parameter	**Value**
Pressure	5,575.13 Pa
Density	0.089 kg/m^3
Velocity profile at altitude	15 m/s

4.1.4 Applied Load

The hull duct wall is subject to hull overpressure on its outer surface and duct-flow-induced pressures on its inner surface. The total pressure on the duct wall is the summation of ambient pressure acting on the hull as provided in Tables 4.4, 4.5, and 4.6, the hull overpressure of 200 Pa on the outer surface, and the static pressure due to air flow on the inner surface (pressure suction), which is variable along the length of the duct. Consequently, the duct experiences in-plane compression forces along most of its length. To determine the duct flow pressures on the inner surface of the duct wall, the principle of conservation of momentum was applied across the propeller disc, which provides the first order prediction of the propeller's pressure and velocity distribution. The classical momentum theory for rotorcraft is based on laws of conservation and assumptions that the flow considered is steady, inviscid, incompressible, irrotational, and quasi-one dimensional. The actuator disc theory [13] is a simple qualitative diagnostic model to study the basic fundamentals of rotary wing aerodynamics. Figure 4.4 represents a ducted propeller system showing the far-field pressure, P_∞, and the velocity at the far field, V_∞.

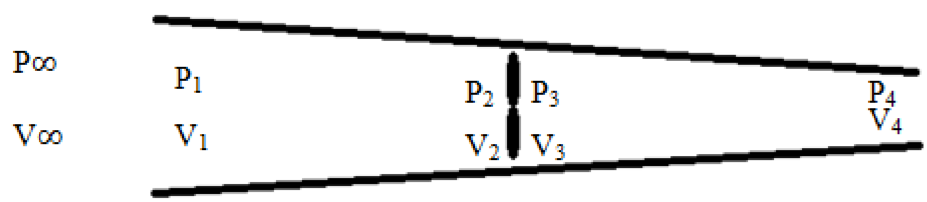

Figure 4.4 Convergent propulsive duct

The conservation of momentum is applied between points ∞ and 2, 1, and 2, and between 3 and 4.

$$P_\infty + \frac{\rho}{2}V_\infty^2 = P_2 + \frac{\rho}{2}V_p^2 \tag{4.2}$$

$$P_1 + \frac{\rho}{2}V_1^2 = P_2 + \frac{\rho}{2}V_p^2 \tag{4.3}$$

$$P_3 + \frac{\rho}{2}V_p^2 = P_4 + \frac{\rho}{2}V_4^2 \tag{4.4}$$

The velocity of air at the propeller is $V_2 = V_3 = V_p$, which is the summation of V_∞, far field velocity and V_i, the induced velocity. V_i at the propeller is given by

$$V_i = -\frac{V_\infty}{2} + \sqrt{\left(\frac{V_\infty}{2}\right)^2 + \frac{T}{2\rho A_p}} \tag{4.5}$$

There is a pressure jump Δp across the propeller disc between point 2 and 3 given by T/A_p, the thrust produced due to propulsion divided by the area at the duct at propeller. For an airship to remain stationary in flight with respect to the ground, the thrust should overcome the drag experienced by the airship, $D_{airship}$. Hence, the thrust is given by

$$T = D_{airship} = \frac{\rho}{2} V_\infty^2 (\pi R^2) C_d \tag{4.6}$$

where V_∞ is the velocity of winds at that altitude. By applying the conservation of momentum across infinity and point 2, P_2 was determined. Furthermore, applying the conservation of momentum between point 1 and 2, the variable pressure along the length of the first section was determined. For the rear section of the duct, P_3, the pressure just after the propeller disc, can be determined by adding the pressure, P_2, i.e. the pressure before the disc, and Δp. The variation in the air pressure through the flow-field is given by the Eqs. (4.2), (4.3), and (4.4) and are plotted in Figure 4.5, 4.6, and 4.7, respectively; is used to determine the pressure as a function of the length of the duct.

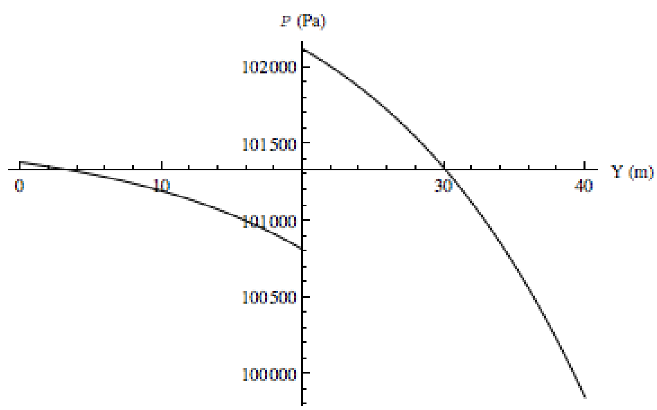

Figure 4.5 Absolute pressure variations on inner wall of the duct at sea Level

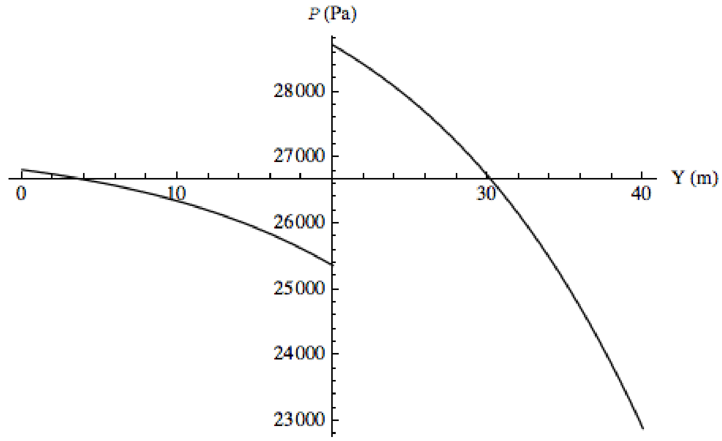

Figure 4.6 Absolute pressure variations on inner wall of the duct at 32.5 kft

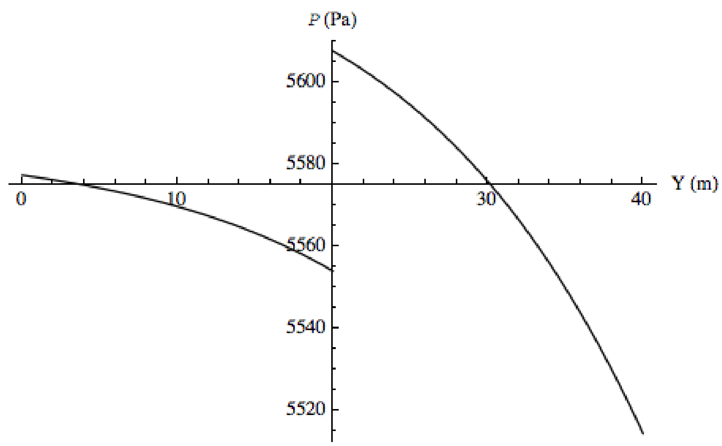

Figure 4.7 Absolute pressure variations on inner wall of the duct at 65 kft

These pressures when added to ambient pressure and hull pressure are used as inputs to the FEM analysis and are given as

<u>Front Part at Sea Level</u>

$$P_{Part\,1} = 45 - \frac{61353.6}{\left(0.000454951y^2 - 0.0712311y + 4.24264\right)^4} \tag{4.7}$$

<u>Rear Part at Sea Level</u>

$$P_{Part\,2} = 1351.67 - \frac{61353.6}{\left(0.000454951y^2 - 0.0712311y + 4.24264\right)^4} \tag{4.8}$$

Front Part at 32.5 kft

$$P_{Part\,1} = 428.182 - \frac{157311}{\left(0.000454951y^2 - 0.0712311y + 4.24264\right)^4} \quad (4.9)$$

Rear Part at 32.5 kft

$$P_{Part\,2} = 3778.49 - \frac{157311}{\left(0.000454951y^2 - 0.0712311y + 4.24264\right)^4} \quad (4.10)$$

Front Part at 65 kft

$$P_{Part\,1} = -189.915 - \frac{2525.55}{\left(0.000454951y^2 - 0.0712311y + 4.24264\right)^4} \quad (4.11)$$

Rear Part at 65 kft

$$P_{Part\,2} = -136.127 - \frac{2525.55}{\left(0.000454951y^2 - 0.0712311y + 4.24264\right)^4} \quad (4.12)$$

By using Equations 4.7 and 4.8, 4.9 and 4.10, and 4.11 and 4.12, the pressure exerted on duct at sea level, 32.5 kft, and 65 kft, respectively, are plotted in Figures 4.8, 4.9, and 4.10, respectively. The pictorial views of pressure exerted on the duct are shown in Figure 4.11, 4.12, and 4.13 for their corresponding operating conditions.

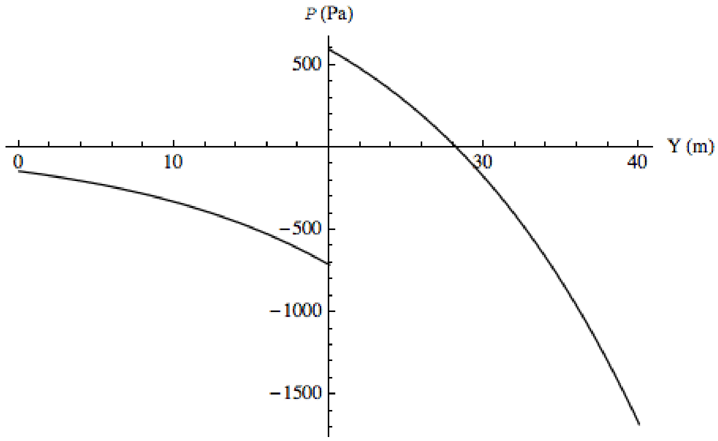

Figure 4.8 Pressure exerted on the convergent propulsive duct at sea level

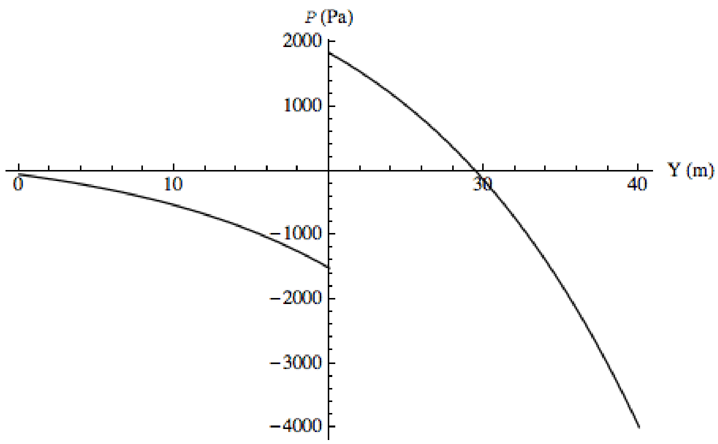

Figure 4.9 Pressure exerted on the convergent propulsive duct at 32.5 kft

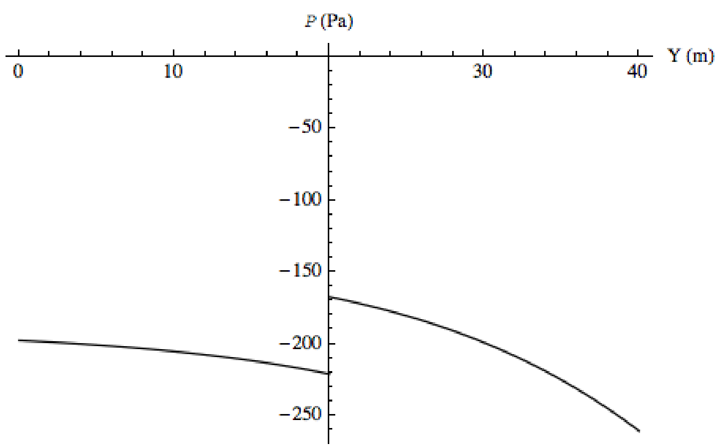

Figure 4.10 Pressure exerted on the convergent propulsive duct at 65 kft

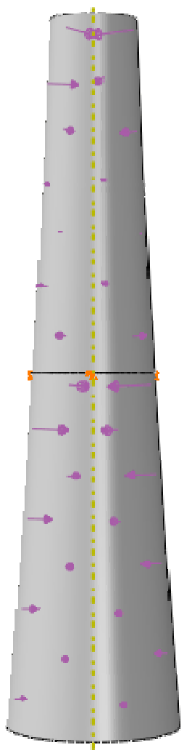

Figure 4.11 Pressure distribution along the length of the duct for at Sea Level

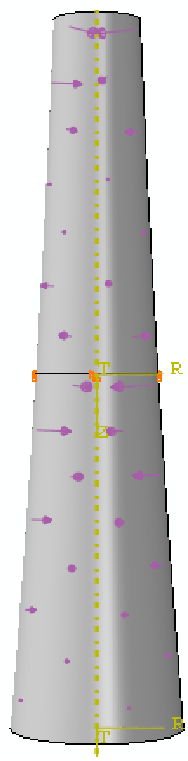

Figure 4.12 Pressure distribution along the length of the duct for 32.5 kft

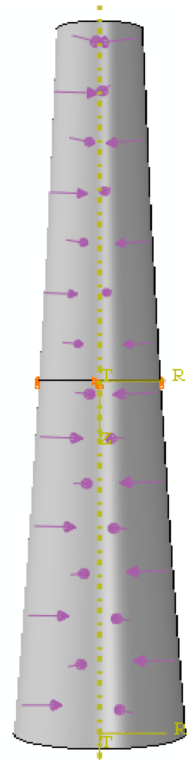

Figure 4.13 Pressure distribution along the length of the duct for 65 kft

In the analysis a lateral pressure loading along the duct is provided; hence ABAQUS determines the buckling factor, for which in this case after considering the margin of safety of 50% is 1.5.

4.1.5 Boundary Conditions

The geometry of duct and the applied loading is axisymmetric. It is known that when a large compressive pressure is applied on the duct, it tends to experience finite radial displacement. To impose free-free boundary conditions in the FEM model, four circumferential nodes were chosen at 0°, 90°, 180° and 270° at the half-length of the duct as shown in Fig. 4.14; the nodes at 0° and 180° degree were constrained along the Y and Z axis, and the nodes at 90° and 270° were constrained along the Y and X axis of the duct. In Fig. 4.14 the Y-axis is perpendicular to the X-Z plane and it points into the plane of the page.

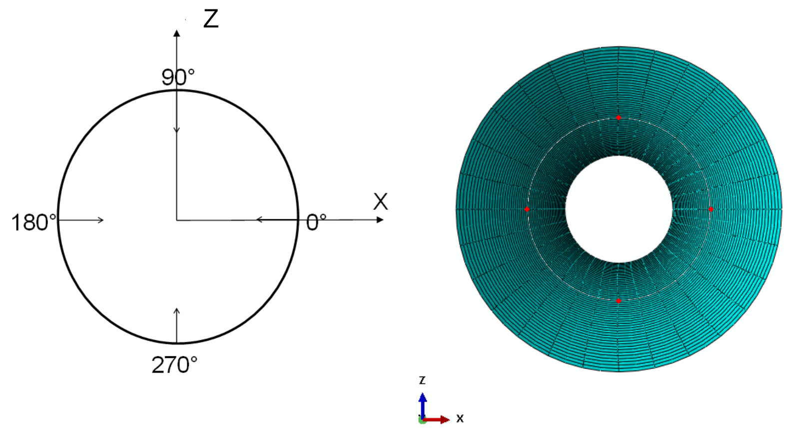

Figure 4.14 Constrained nodes to simulate free-free boundary condition

4.1.6 Mesh Refinement Study

A mesh refinement study was conducted in order to determine the required level of discretization for solution convergence. S8R thick shell elements that include through-the-thickness shear were used for composite sandwich. The S8R elements are 8 node shell elements that utilize quadratic shape functions that accurately accounts for moments and shear. Such elements result in higher order of strain variation with each element, and faster solution convergence with minimal elements as compared to S4R elements. A mesh refinement study was performed for the first buckling mode until the solution converged to a percentage residue of less than 0.02% for the foam-only duct, graphite/epoxy laminate-only duct, and composite sandwich duct, each at sea level, 32.5 kft, and 65 kft. Then the same mesh was used for the optimization procedure.

4.1.6.1 Mesh Refinement Study for the Airship Operating at Sea Level

A mesh refinement study was done for foam-only, graphite/epoxy laminate-only, and composite sandwich duct, respectively for the airship operating at sea level.

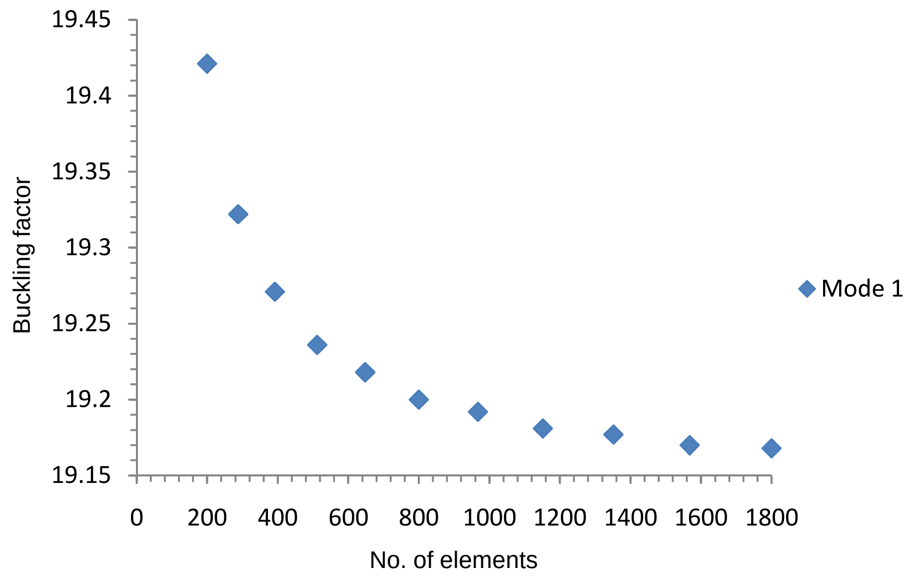

Figure 4.15 Mesh refinement study performed for 1st buckling mode for foam-only duct, t_f=200 mm

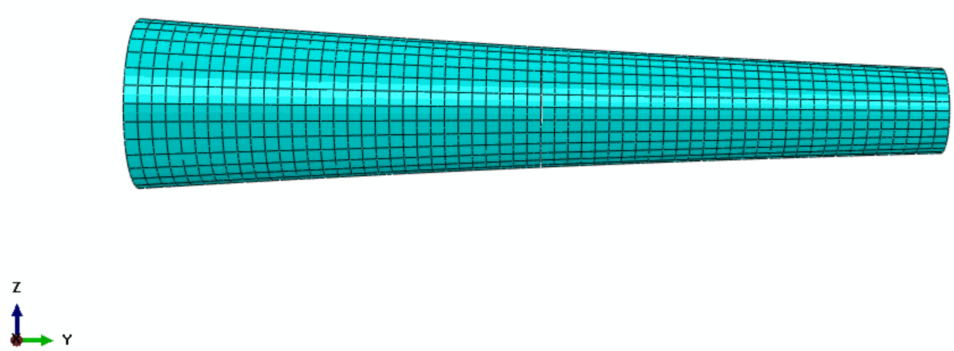

Figure 4.16 Mesh of 1800 elements for foam-only duct

The solution convergence study reveals that a minimum of 1800 number of elements are sufficient for a residual percentage lower than 0.02% for the 1st buckling mode for foam-only duct of the airship operating at sea level.

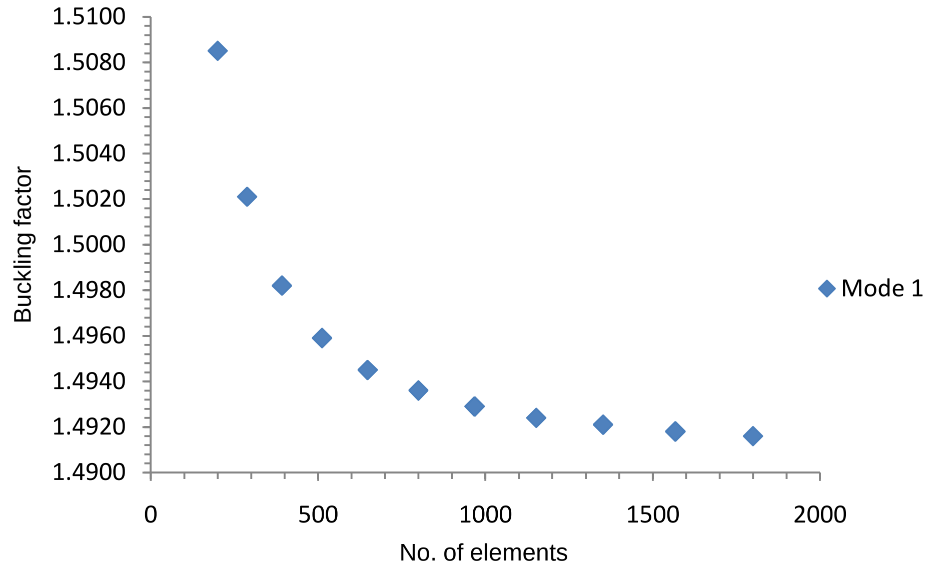

Figure 4.17 Mesh refinement study performed for 1st buckling mode for graphite/epoxy laminate-only duct $[90_{60}]_T$

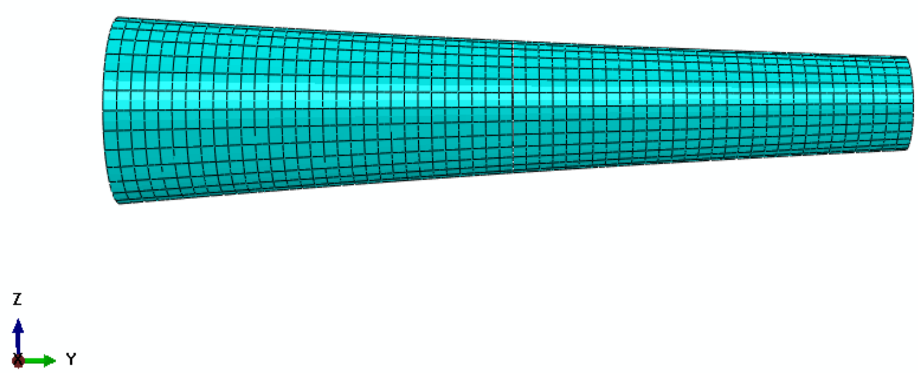

Figure 4.18 Mesh of 1800 elements for graphite/epoxy laminate-only duct

The solution convergence study reveals that a minimum of 1800 number of elements are sufficient for a residual percentage lower than 0.02% for the 1st buckling mode for graphite/epoxy laminate-only duct of the airship operating at sea level.

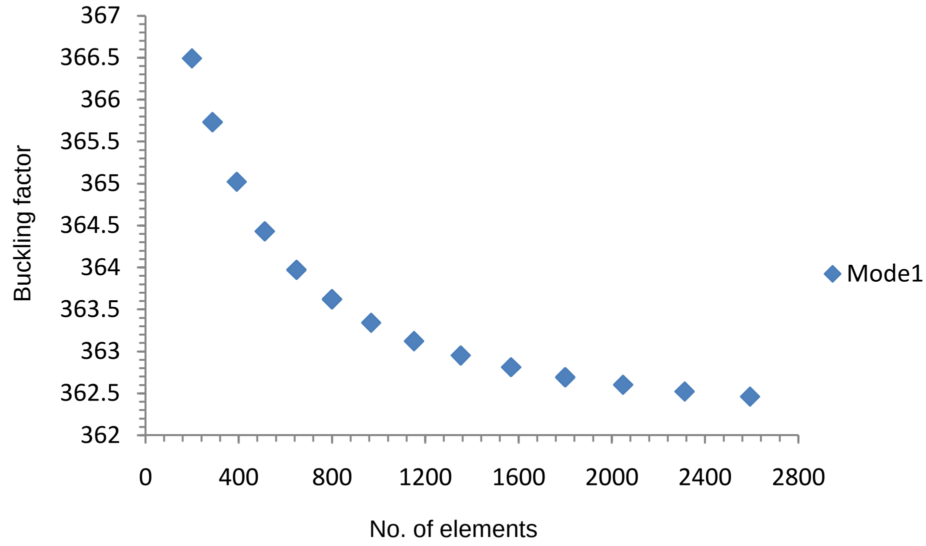

Figure 4.19 Mesh refinement study performed for 1st buckling mode for composite sandwich duct $[90_{30}/F/90_{30}]_T$, t_f=83.816 mm

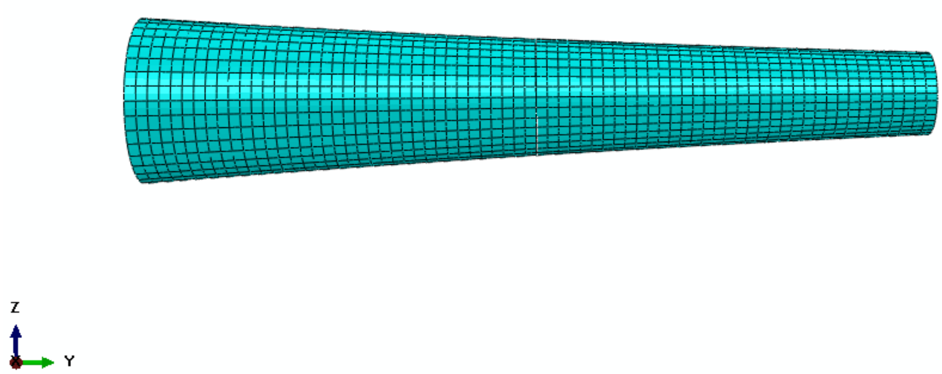

Figure 4.20 Mesh of 2592 elements for composite sandwich duct

The solution convergence study reveals that a minimum of 2592 number of elements are sufficient for a residual percentage lower than 0.02% for the 1st buckling mode for composite sandwich duct of the airship operating at sea level.

4.1.6.2 Mesh Refinement Study for the Airship Operating at 32.5 kft

A mesh refinement study was done for foam-only, graphite/epoxy laminate-only duct and composite sandwich duct respectively for the airship operating at 32.5 kft.

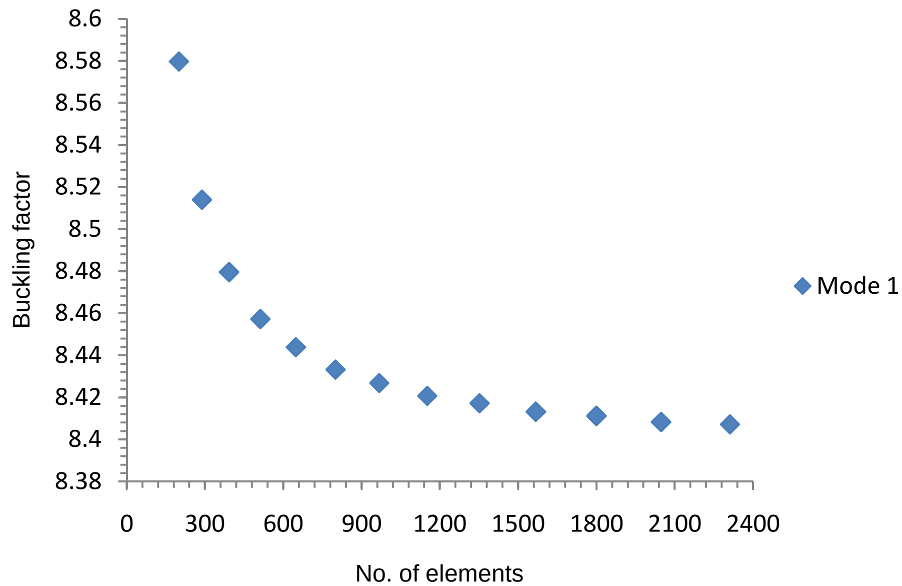

Figure 4.21 Mesh refinement study performed for 1st buckling mode for foam-only duct, t_f=200 mm

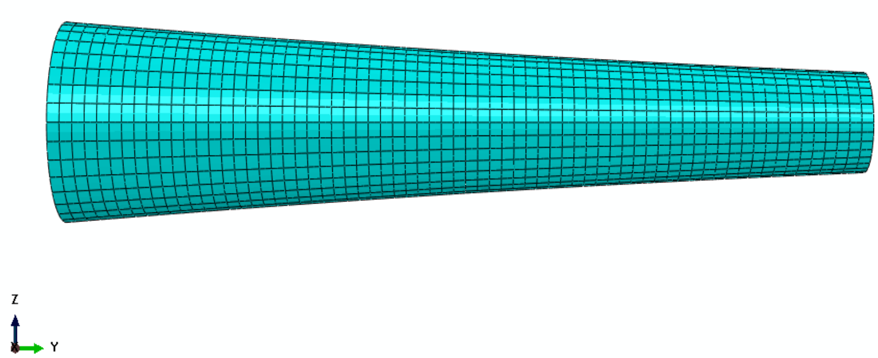

Figure 4.22 Mesh of 2312 elements for foam-only duct

The solution convergence study reveals that a minimum of 2312 number of elements are sufficient for a residual percentage lower than 0.02% for the 1st buckling mode for foam-only duct of the airship operating at 32.5 kft.

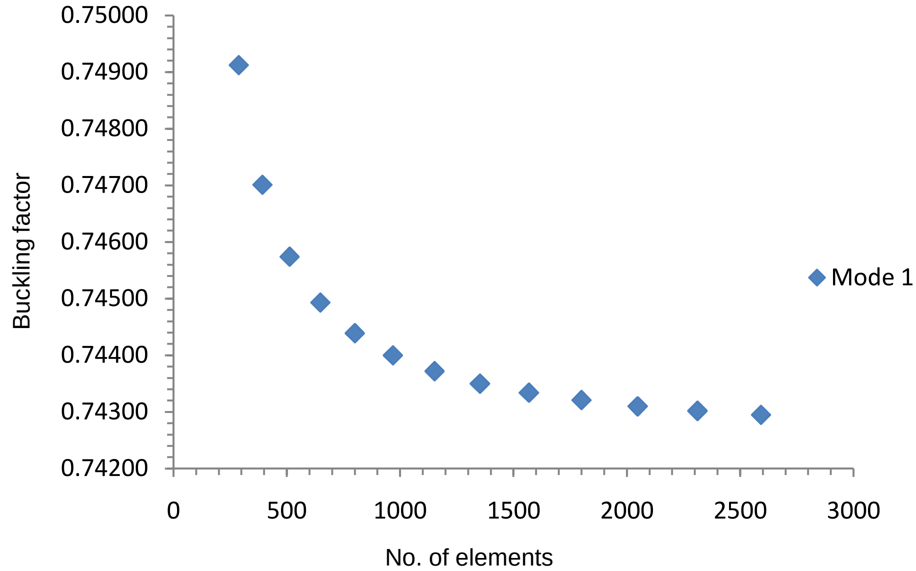

Figure 4.23 Mesh refinement study performed for 1st buckling mode for graphite/epoxy laminate-only duct $[90_{60}]_T$

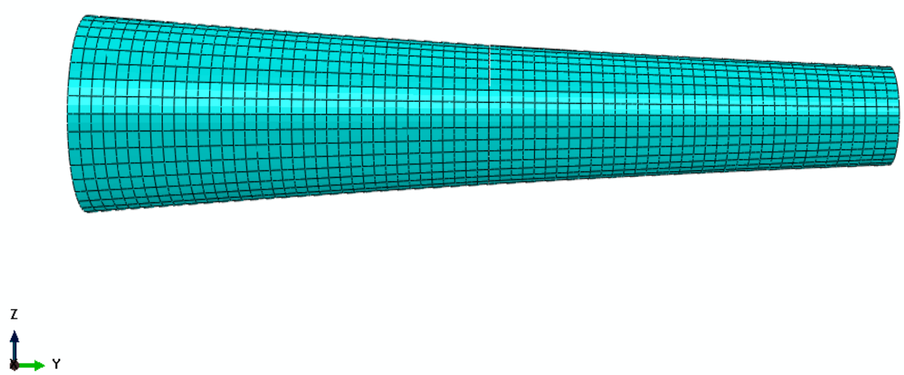

Figure 4.24 Mesh of 2592 elements for graphite/epoxy laminate-only duct $[90_{60}]_T$

The solution convergence study reveals that a minimum of 2592 number of elements are sufficient for a residual percentage lower than 0.02% for the 1st buckling mode for graphite/epoxy laminate-only duct of the airship operating at 32.5 kft.

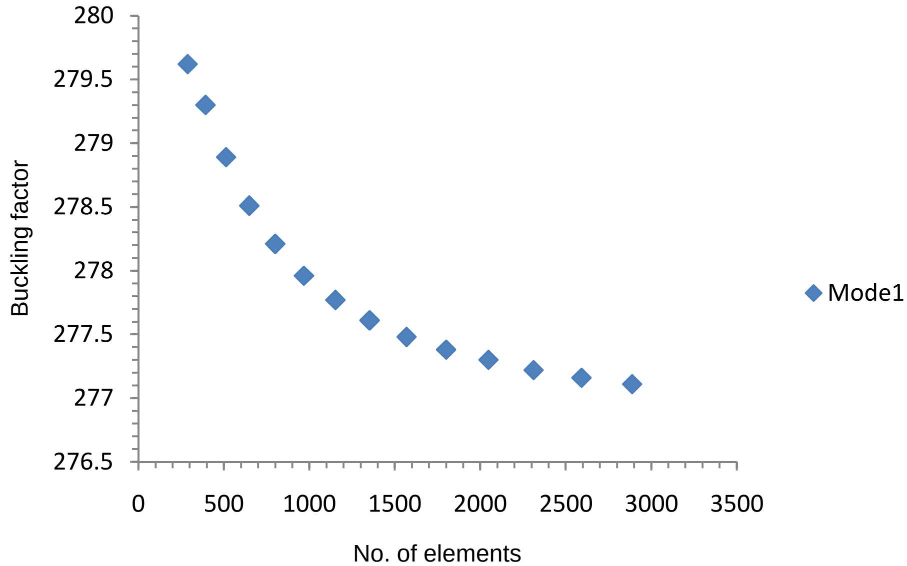

Figure 4.25 Mesh refinement study performed for 1st buckling mode for composite sandwich duct $[90_{38}/F/90_{38}]_T$, t_f=109.341 mm

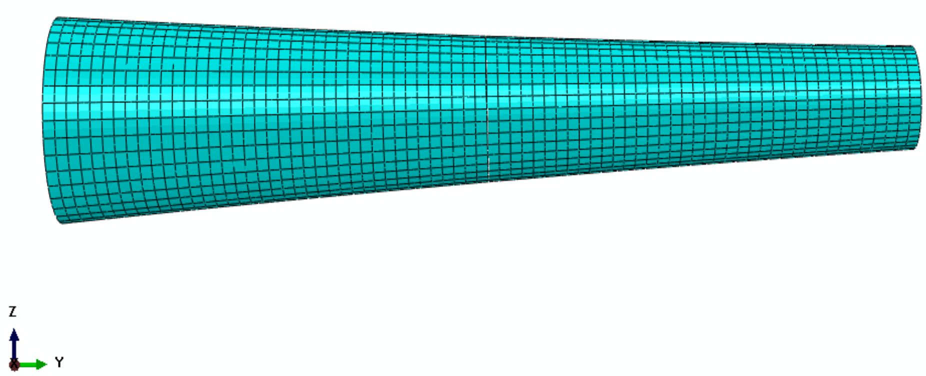

Figure 4.26 Mesh of 2888 elements for composite sandwich duct

The solution convergence study reveals that a minimum of 2888 number of elements are sufficient for a residual percentage lower than 0.02% for the 1st buckling mode for composite sandwich duct of the airship operating at 32.5 kft

4.1.6.3 Mesh Refinement Study for the Airship Operating at 65 kft

A mesh refinement study was done for foam-only, graphite/epoxy laminate-only duct and composite sandwich duct respectively for the airship operating at 65 kft.

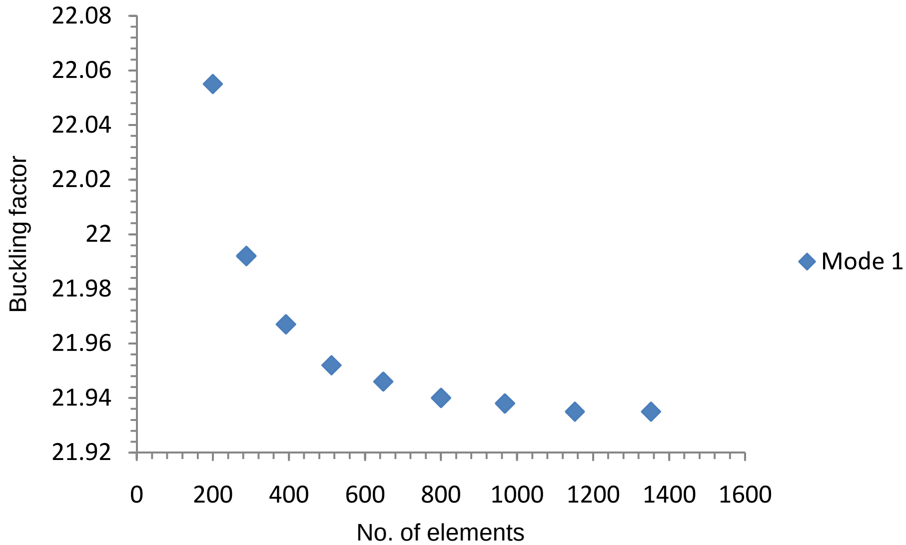

Figure 4.27 Mesh refinement study performed for 1st buckling mode for foam-only duct, t_f=200 mm

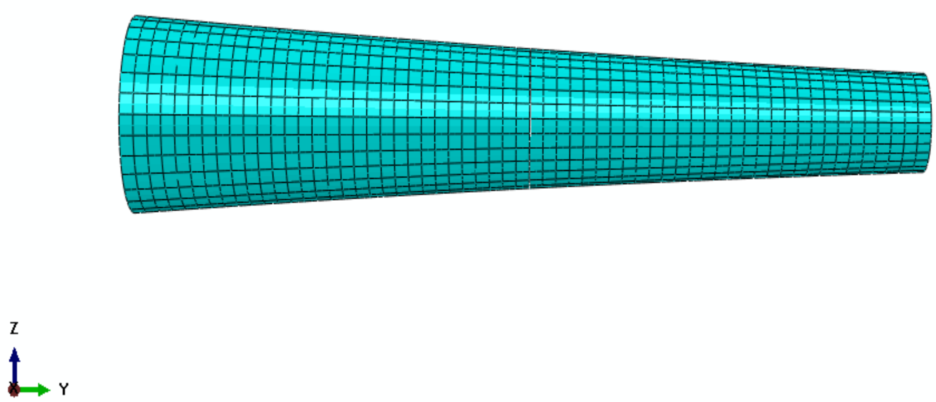

Figure 4.28 Mesh of 1800 elements for foam-only duct

The solution convergence study reveals that a minimum of 1800 number of elements are sufficient for a residual percentage lower than 0.02% for the 1st buckling mode for foam-duct of the airship operating at 65 kft.

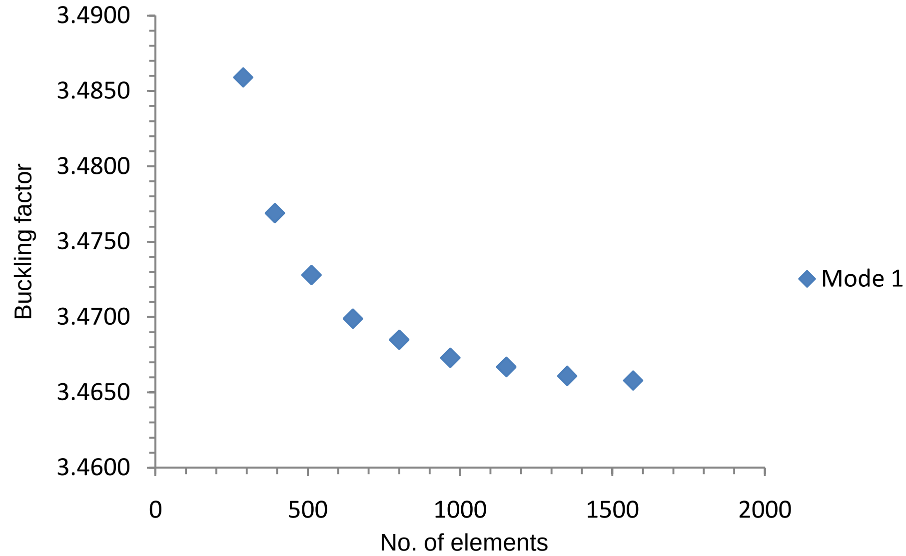

Figure 4.29 Mesh refinement study performed for 1st buckling mode for graphite/epoxy laminate-only duct $[90_{60}]_T$

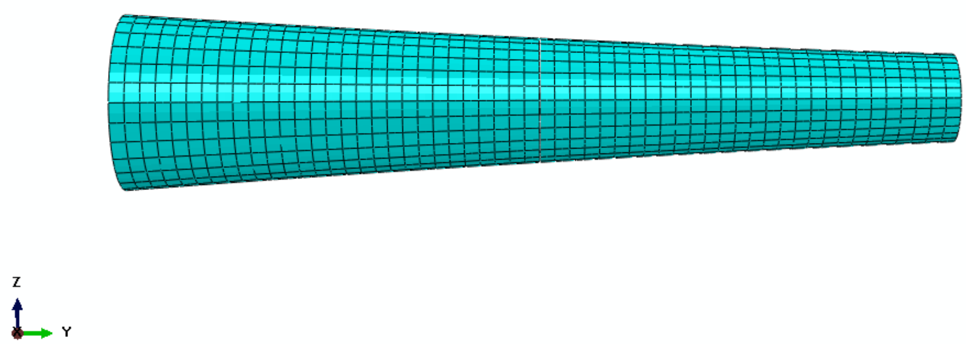

Figure 4.30 Mesh of 1568 elements for graphite/epoxy laminate-only duct $[90_{60}]_T$

The solution convergence study reveals that a minimum of 1568 number of elements are sufficient for a residual percentage lower than 0.02% for the 1st buckling mode for graphite/epoxy laminate-only duct of the airship operating at 65 kft.

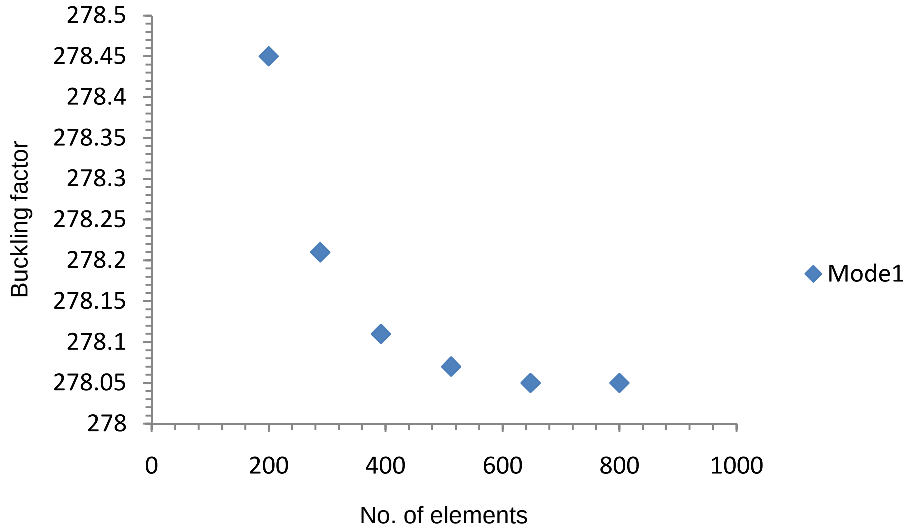

Figure 4.31 Mesh refinement study performed for 1st buckling mode for composite sandwich duct $[90_{22}/F/90_{22}]_T$, t_f=71.445 mm

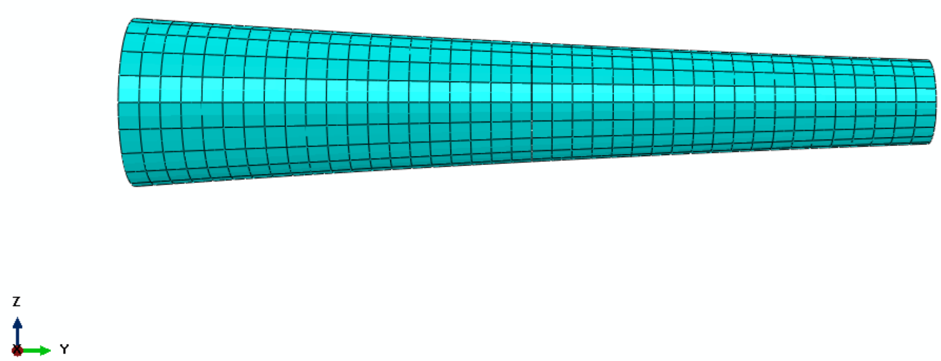

Figure 4.32 Mesh of 800 elements for composite sandwich duct

The solution convergence study reveals that a minimum of 800 number of elements are sufficient for a residual percentage lower than 0.02% for the 1st buckling mode for composite sandwich duct of the airship operating at 65 kft.

4.2 FEM-Based Structural Optimization

To achieve an optimal configuration for the composite sandwich duct operating at sea level, 32.5 kft, and 65 kft, a sizing study was undertaken for the following cases: (a) foam-only duct, (b) a graphite/epoxy laminate-only duct, and (c) a sandwich composite duct with graphite/epoxy face sheets and a foam core. For the graphite/epoxy laminate-only duct the orientation of plies were selected to be either 0˚ or 90˚; hence the stacking sequences analyzed in this study were $[90_n]_T$, $[0_n]_T$ and $[(90/0)_n]_T$. For the case of a sandwich composite duct, the layups investigated are provided in Table 4.7.

Table 4.7 Sandwich layups of interest

One-ply sandwich	$[90/F/90]_T$ $[0/F/0]_T$ $[90/F/0]_T$
Two-ply sandwich	$[90_2/F/90_2]_T$ $[0_2/F/0_2]_T$ $[90_2/F/0_2]_T$ $[90/0/F/90/0]_T$
Three-ply sandwich	$[90_3/F/90_3]_T$ $[0_3/F/0_3]_T$ $[90_3/F/0_3]_T$ $[90/0/90/F/90/0/90]_T$
Four-ply sandwich	$[90_4/F/90_4]_T$ $[0_4/F/0_4]_T$ $[90_4/F/0_4]_T$ $[90/0/90/0/F/0/90/0/90]_T$

* F indicates for foam core.

An iterative method was utilized to solve for minimum foam thickness (when considering a foam-only or sandwich structure) and the minimum number of plies (when considering a composite laminate structure) required to meet the stability condition. The iteration involved determining an interpolation function for buckling pressure as a function of foam thickness or number of plies. The interpolation function was generated by making three initial guesses for the foam thickness or number of plies. ABAQUS was then used to solve for the buckling factor. These three points were used to find a quadratic function for the buckling factor, which was solved for foam thickness or number of plies at buckling factor of 1.5. If for the solved value ABAQUS did not return the buckling factor within the tolerance of 1.5±0.0005, the process was repeated using the solved value and two more nearby points. This tolerance was chosen as it was acceptably close to the desired buckling factor. When solving for the number of plies the solution was rounded up to the nearest whole number.

A structural optimization for minimum weight solution was then conducted for all the cases explained above for the airship operating at sea level, 32.5 kft and 65 kft.

4.2.1 Structural Optimization of Duct of the Airship Operating at Sea Level

4.2.1.1 Sizing of Foam-Only Duct

The sizing of foam-only duct was performed first. The study showed that for the foam-only duct, the required foam thickness was 83.816 mm which resulted in buckling factor of 1.4999, and a corresponding duct mass of 6457.790 kg.

The sizing procedure showing the determination of a quadratic function, for finding minimum foam thickness for duct at sea level is given in Figure 4.33.

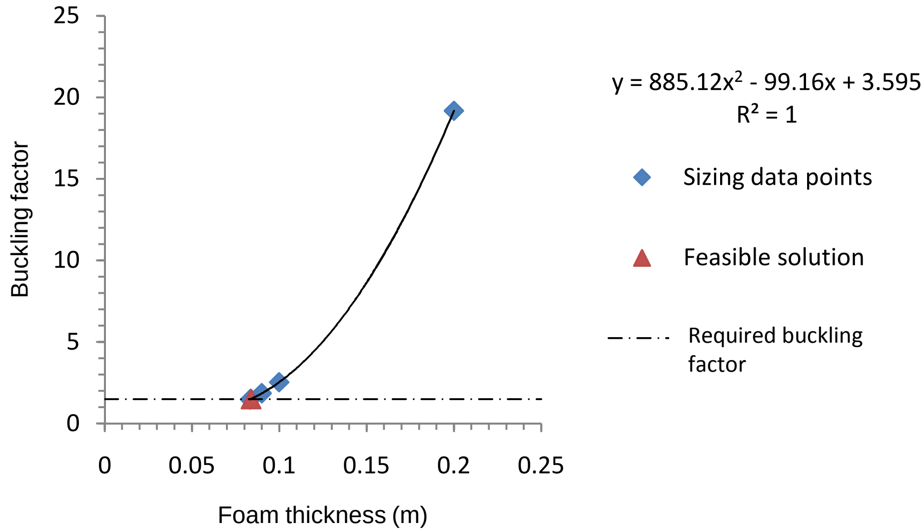

Figure 4.33 Buckling factor as a function of foam thickness for a foam-only duct.

4.2.1.2 Sizing of Graphite/Epoxy Laminate-Only Duct

The next step was to perform a sizing study of a composite duct made of graphite/epoxy laminate. The minimum number of plies required to prevent buckling, with their corresponding buckling factors and masses are presented in Table 4.8.

Table 4.8 Optimized graphite/epoxy laminate-only duct configurations at sea level

Fiber Orientation	Number of plies (n)	Buckling factor	Mass (kg)
$[90_n]_T$	60	1.4916	9187.880
$[0_n]_T$	140	1.5116	21438.400
$[(90/0)_n]_T$	37	1.5135	11331.700

The sizing procedure showing the determination of a quadratic function, for finding the minimum number of plies needed to satisfy the stability constraint for the layups $[90_n]_T$, $[0_n]_T$, and $[(90/0)_n]_T$ is given in Figures 4.34, 4.35, and 4.36, respectively.

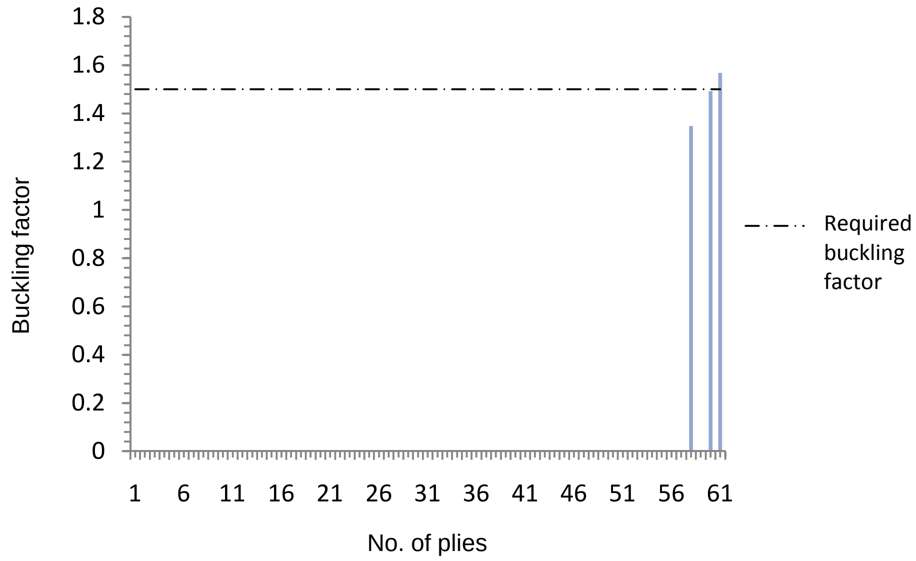

Figure 4.34 Buckling factor as a function of no. of plies for the layup $[90_n]_T$

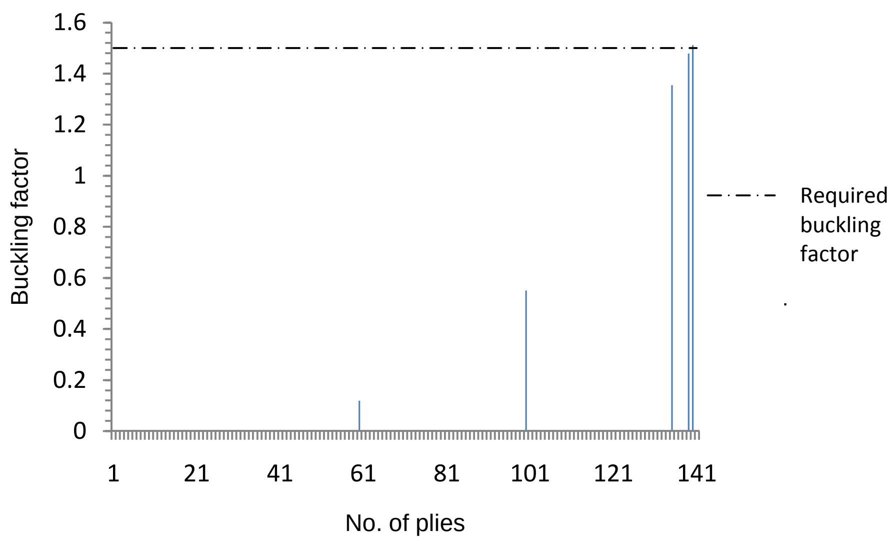

Figure 4.35 Buckling factor as a function of no. of plies for the layup $[0_n]_T$

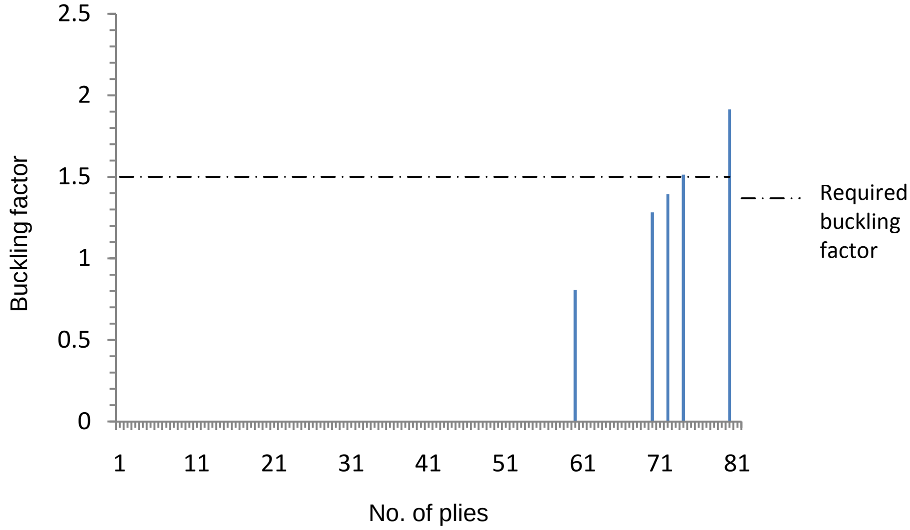

Figure 4.36 Buckling factor as a function of no. of plies for the layup $[(90/0)_n]_T$

4.2.1.3 Optimization of Graphite/Epoxy Laminate-Only Duct

After iterating for minimum number of plies for each layup, an optimization study was conducted to find an optimum minimum weight solution from the feasible set of solutions shown in Figure 4.37.

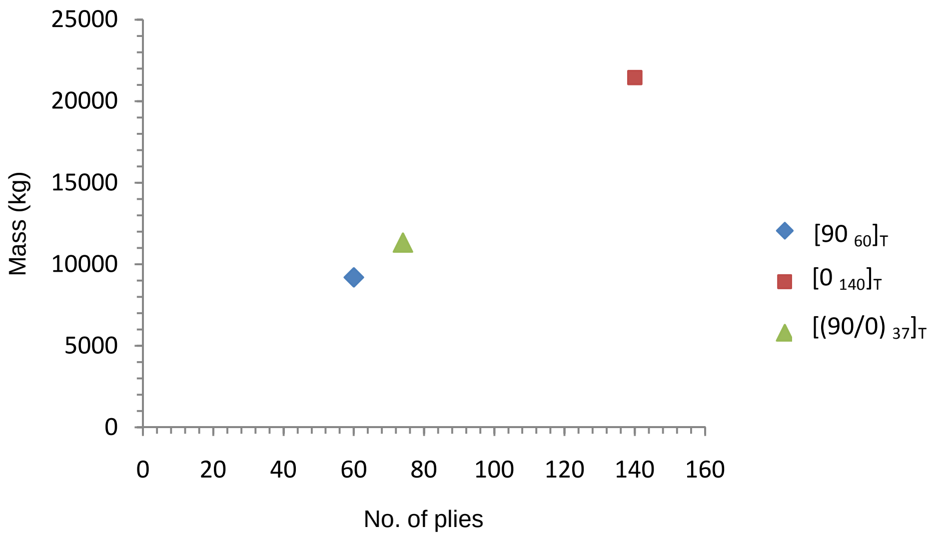

Figure 4.37 Optimization for minimum mass for graphite/epoxy laminate-only duct

Based upon the results shown in Figure. 4.37, the optimum composite layup for the propulsive duct was $[90_{60}]_T$ for which the minimum duct mass was 9187.880 kg.

4.2.1.4 Sizing of Composite Sandwich Duct

Sizing studies were conducted in ABAQUS for the sandwich layups as provided in Table 4.7. The number of plies in a face sheet was increased until the minimum mass of the latest configuration exceeded the minimum mass obtained in the previous configuration, whereupon the minimization process was ended. For this case, the mass of the one-ply sandwich layup was greater than two-ply sandwich layup; hence the iteration process was continued. However, the mass of the two-ply sandwich layup was less than three-ply sandwich layup; hence the iteration process was ended. The sizing results for an airship operating at sea level are shown in Table 4.9.

Table 4.9 Optimized composite sandwich duct configurations for airship operating at sea level

Sandwich Layup	Foam thickness(mm)	Buckling factor	Mass (kg)
$[90/F/90]_T$	23.898	1.5001	2147.550
$[0/F/0]_T$	63.350	1.4999	5182.100
$[90/F/0]_T$	43.400	1.5003	3876.630
$[90_2/F/90_2]_T$	16.787	1.5000	1905.960
$[0_2/F/0_2]_T$	51.856	1.4997	4607.880
$[90_2/F/0_2]_T$	37.760	1.4999	3521.830
$[90/0/F/90/0]_T$	22.549	1.5000	2349.910
$[90_3/F/90_3]_T$	13.518	1.5001	1960.310
$[0_3/F/0_3]_T$	44.546	1.5000	4350.940
$[90_3/F/0_3]_T$	32.509	1.5001	3423.560
$[90/0/90/F/90/0/90]_T$	16.152	1.5000	2163.260

The sizing procedure showing the determination of a quadratic function, for finding minimum foam thickness for composite sandwich ducts for the layups provided in Table 4.7 are given in Figures 4.38 to 4.48.

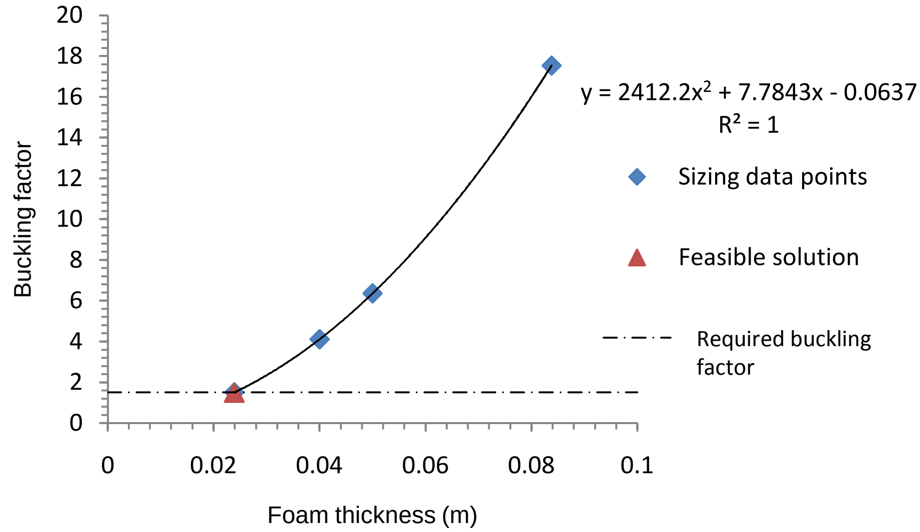

Figure 4.38 Buckling factor as a function of foam thickness for a composite sandwich layup [90/F/90]$_T$

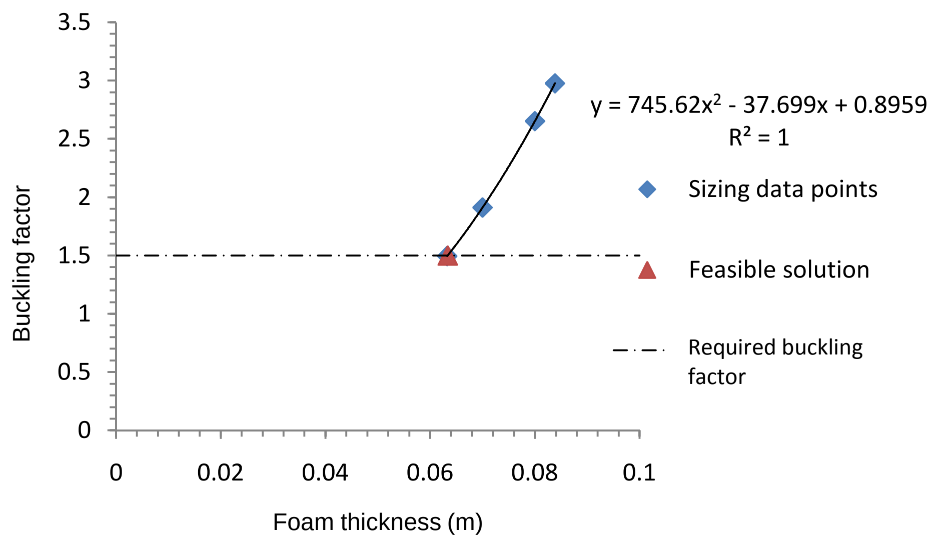

Figure 4.39 Buckling factor as a function of foam thickness for composite sandwich [0/F/0]$_T$

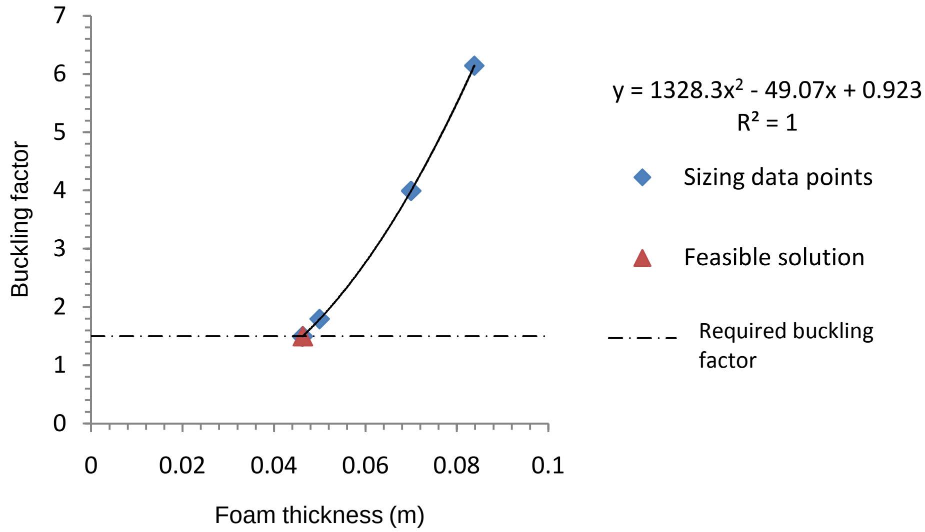

Figure 4.40 Buckling factor as a function of foam thickness for composite sandwich $[90/F/0]_T$

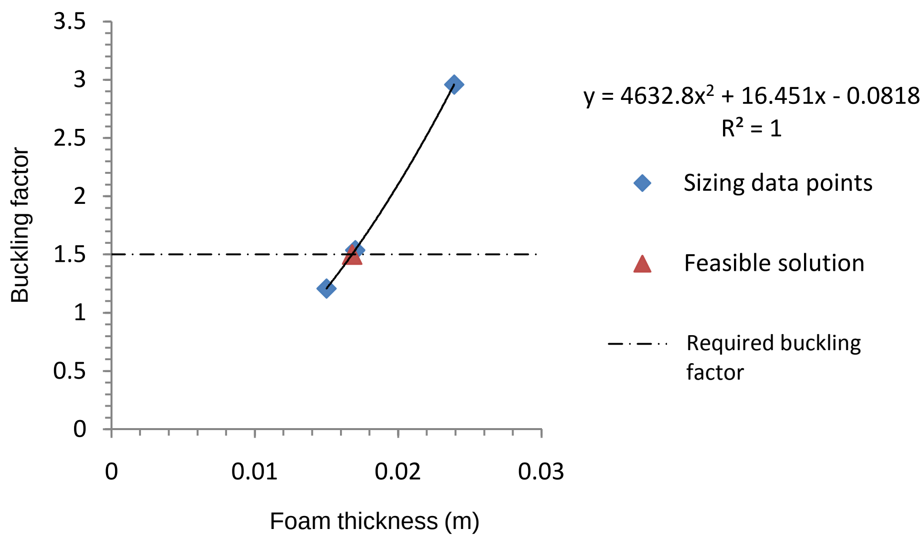

Figure 4.41 Buckling factor as a function of foam thickness for a composite sandwich composite of $[90_2/F/90_2]_T$

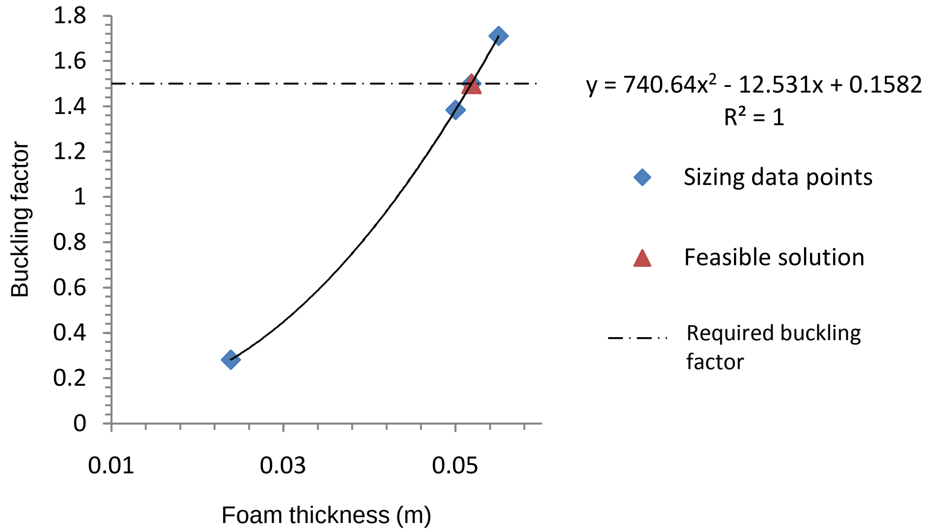

Figure 4.42 Buckling factor as a function of foam thickness for a composite sandwich layup of $[0_2/F/0_2]_T$

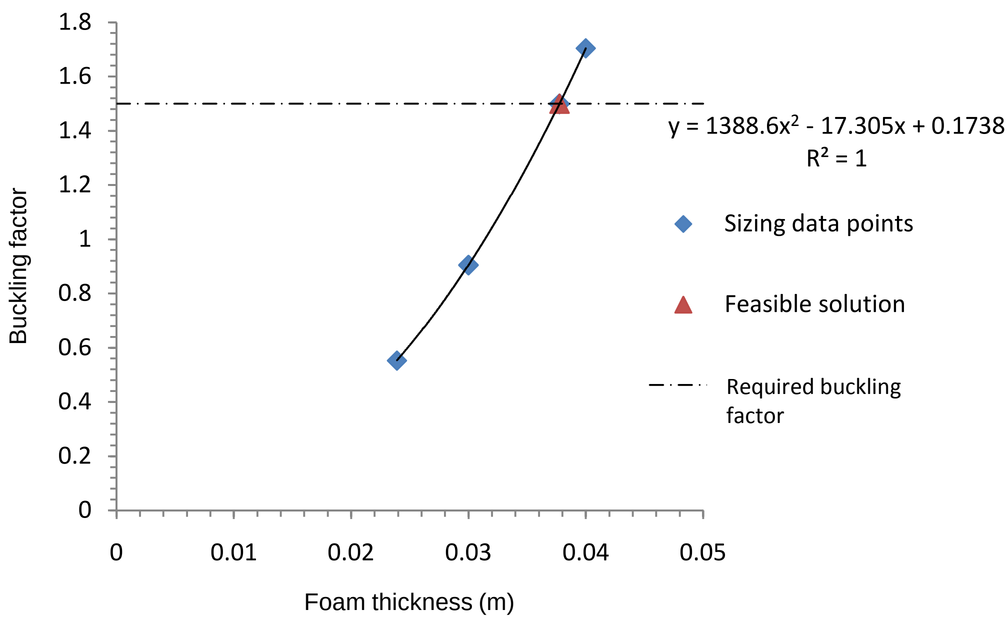

Figure 4.43 Buckling factor as a function of foam thickness for a composite sandwich layup of $[90_2/F/0_2]_T$

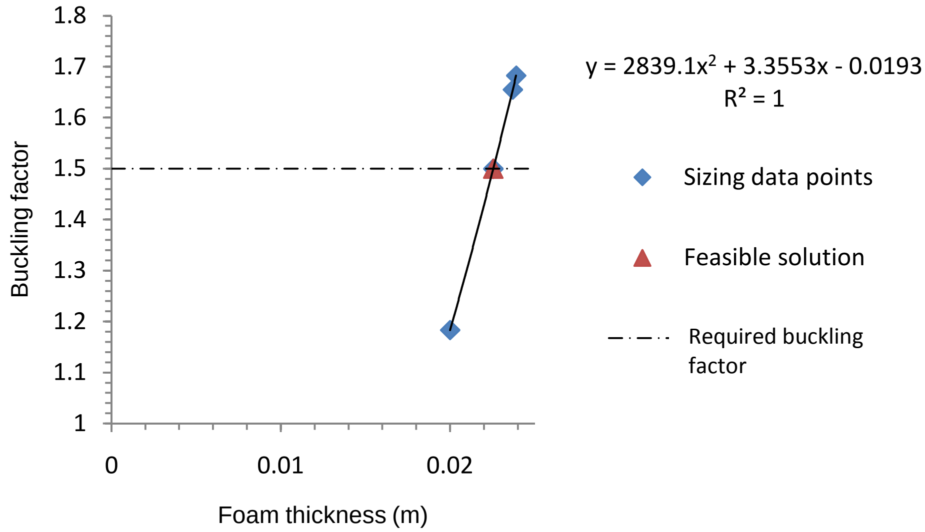

Figure 4.44 Buckling factor as a function of foam thickness for a composite sandwich layup of $[90/0/F/90/0]_T$

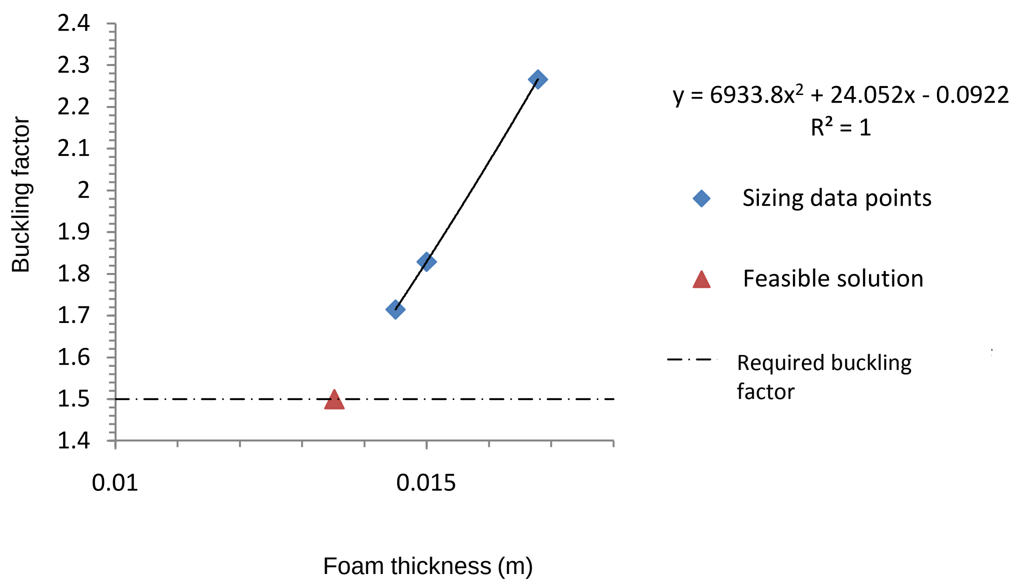

Figure 4.45 Buckling factor as a function of foam thickness for a composite sandwich layup of $[90_3/F/90_3]_T$

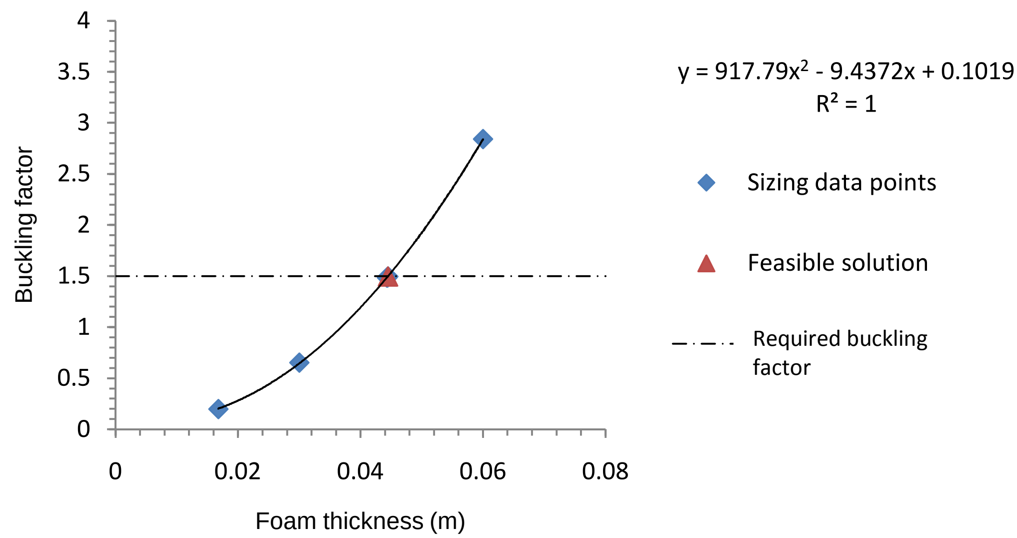

Figure 4.46 Buckling factor as a function of foam thickness for a composite sandwich layup of $[0_3/F/0_3]_T$

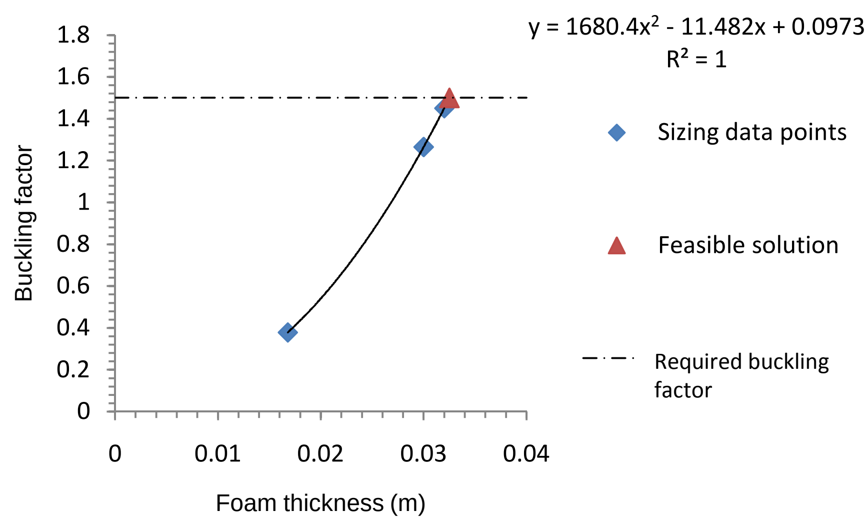

Figure 4.47 Buckling factor as a function of foam thickness for a composite sandwich layup of $[90_3/F/0_3]_T$

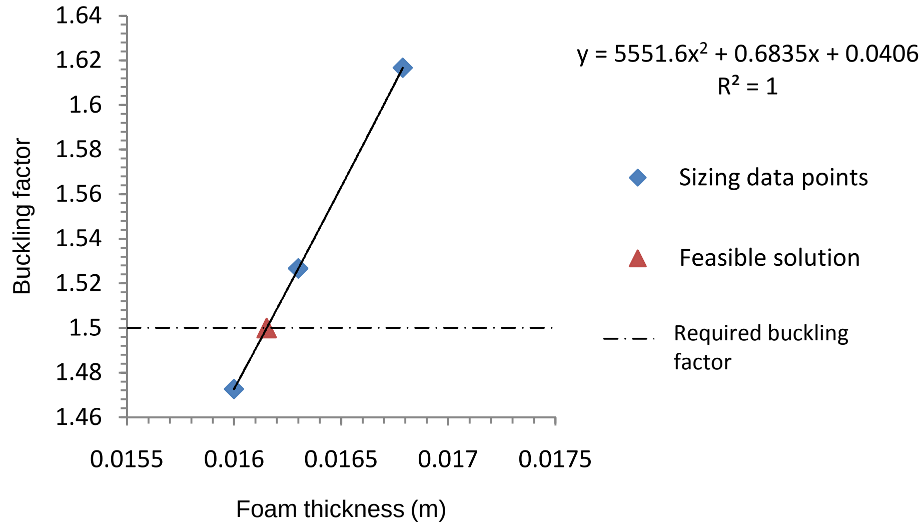

Figure 4.48 Buckling factor as a function of foam thickness for a composite sandwich layup of $[90/0/90/F/90/0/90]_T$

4.2.1.5 Optimization of Composite Sandwich Duct

After sizing for foam for each sandwich layup, an optimization study was conducted to find an optimum minimum weight solution from the feasible set of solutions obtained in the previous section. The feasible sets of solutions are compared in Figure 4.49.

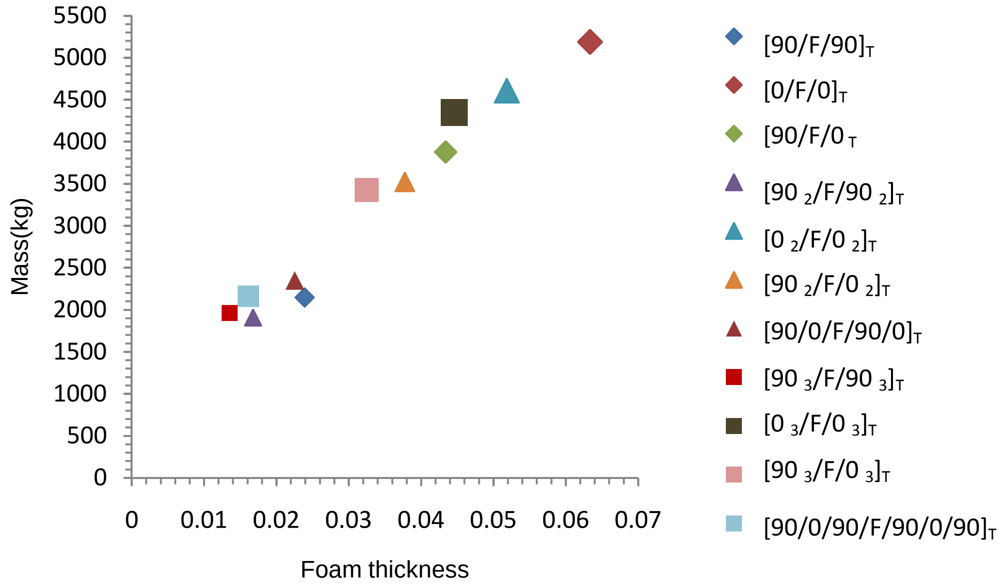

Figure 4.49 Optimization for minimum mass for composite sandwich duct

Based upon the results shown in Figure. 4.49, the optimum sandwich composite layup for the propulsive duct was $[90_2/F/90_2]_T$, t_f=16.174 mm for which the minimum duct mass was 1905.960 kg.

The same procedure was applied to find the optimum layup of composite sandwich for airship operating at 32.5 kft and 65 kft.

4.2.2 Structural Optimization of Duct of the Airship Operating at 32.5 kft

4.2.2.1 Sizing of Foam-Only Duct

The sizing of foam-only duct was performed first. The study showed that for the foam-only duct, the required foam thickness was 109.341 mm which resulted in buckling factor of 1.5005, and a corresponding duct mass of 8424.420 kg.

The sizing procedure showing the determination of a quadratic function, for finding minimum foam thickness for duct at 32.5 kft above sea level is given in Figure 4.50.

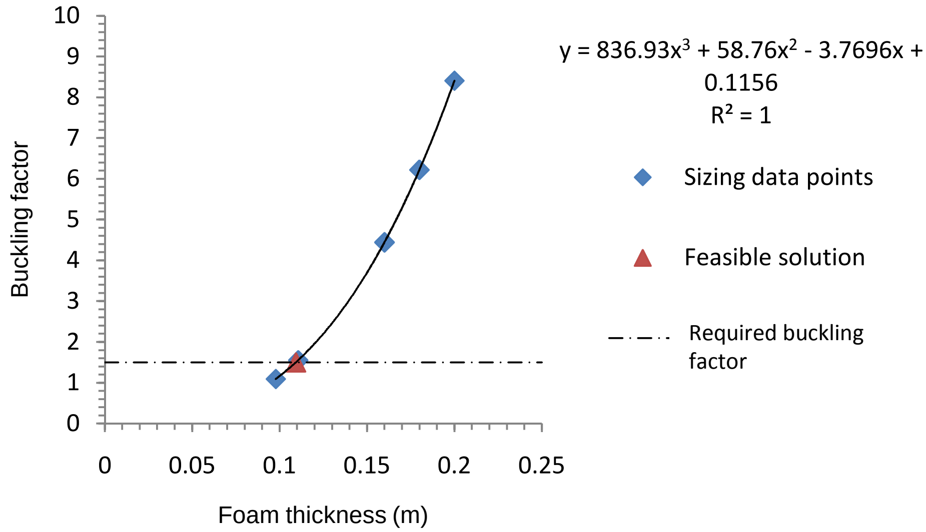

Figure 4.50 Buckling factor as a function of foam thickness for a foam-only duct.

4.2.2.2 Sizing of Graphite/Epoxy Laminate-Only Duct

The next step was to perform a sizing study of a composite duct made of graphite/epoxy laminate. The minimum number of plies required to prevent buckling, with their corresponding buckling factors and masses are presented in Table 4.10. The sizing procedure showing the determination of a quadratic function, for finding the minimum number of plies needed to satisfy the stability constraint for the layups $[90_n]_T$, $[0_n]_T$, and $[(90/0)_n]_T$ is given in Figures 4.51, 4.52, and 4.53, respectively.

Table 4.10 Optimized graphite/epoxy laminate-only duct configurations at 32.5 kft

Fiber Orientation	Number of plies (n)	Buckling factor	Mass (kg)
$[90_n]_T$	76	1.4978	11638.0
$[0_n]_T$	176	1.5103	26951.100
$[(90/0)_n]_T$	47	1.4603	14394.40

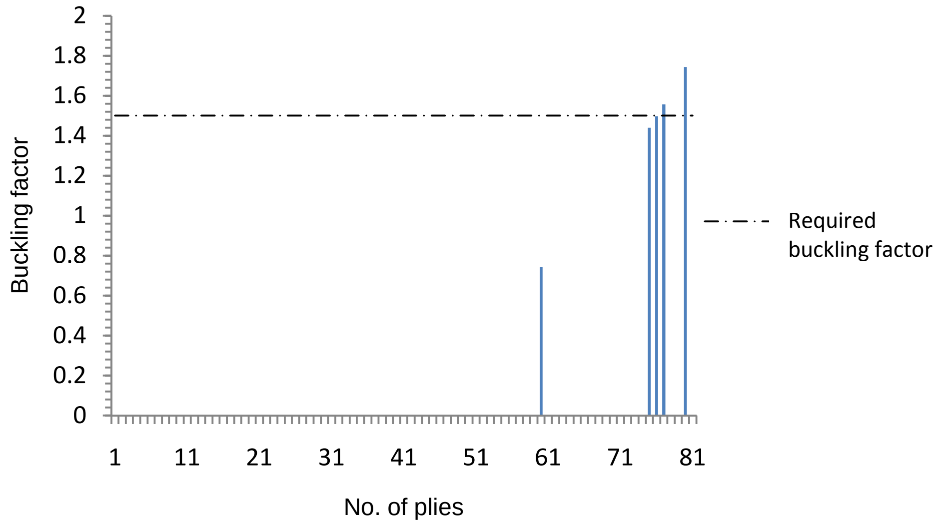

Figure 4.51 Buckling factor as a function of no. of plies for the layups $[90_n]_T$

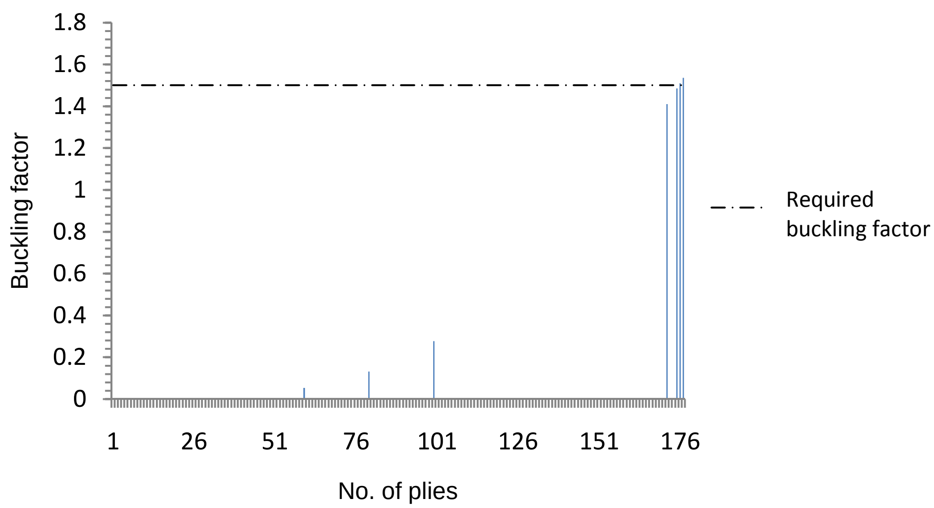

Figure 4.52 Buckling factor as a function of no. of plies for the layups $[0_n]_T$

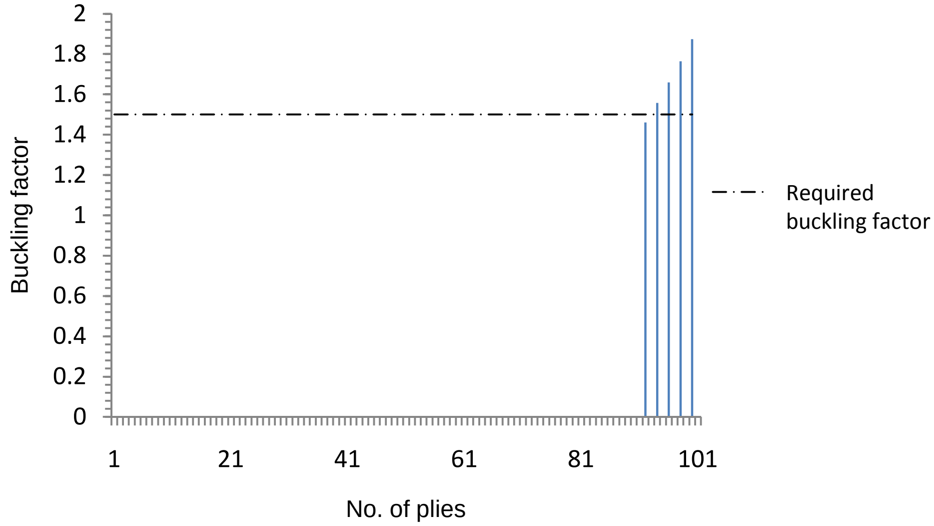

Figure 4.53 Buckling factor as a function of no. of plies for the layups $[(90/0)_n]_T$

4.2.2.3 Optimization of Graphite/Epoxy Laminate-Only Duct

After iterating for minimum number of plies for each layup, an optimization study was conducted to find an optimum minimum weight solution from the feasible set of solutions shown in Figure 4.54.

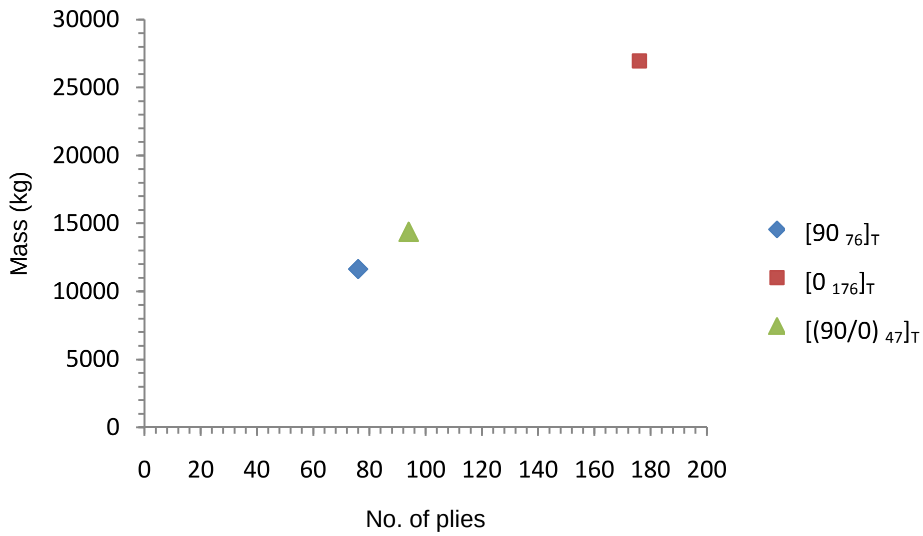

Figure 4.54 Optimization for minimum mass for graphite/epoxy laminate-only duct

Based upon the results shown in Figure. 4.54, the optimum composite layup for the propulsive duct was $[90_{76}]_T$ for which the minimum duct mass was 11638.0 kg.

4.2.2.4 Sizing of Composite Sandwich Duct

Sizing studies were conducted in ABAQUS for the sandwich layups as provided in Table 4.7 for airship operating at 32.5 kft. The number of plies in a face sheet was increased until the minimum mass of the latest configuration exceeded the minimum mass obtained in the previous configuration, whereupon the minimization process was ended. Unlike the previous case, three plies in the face sheet were needed before an increase in mass was observed as compared to face sheets with one additional ply. The sizing results are shown in Table 4.11.

The sizing procedure showing the determination of a quadratic function, for finding minimum foam thickness for composite sandwich ducts for the layups provided in Table 4.7 are given in Figures 4.55 to 4.69.

Table 4.11 Optimized composite sandwich duct configurations for airship operating at 32.5kft

Sandwich Layup	Foam thickness(mm)	Buckling factor	Mass (kg)
$[90/F/90]_T$	36.255	1.5000	3099.610
$[0/F/0]_T$	85.174	1.5004	6868.720
$[90/F/0]_T$	63.321	1.4995	5185.040
$[90_2/F/90_2]_T$	25.528	1.4998	2579.400
$[0_2/F/0_2]_T$	71.140	1.5002	6093.670
$[90_2/F/0_2]_T$	52.145	1.5000	4630.150
$[90/0/F/90/0]_T$	32.588	1.4999	3123.410
$[90_3/F/90_3]_T$	20.515	1.5000	2499.450
$[0_3/F/0_3]_T$	45.276	1.5002	5681.460
$[90_3/F/0_3]_T$	61.815	1.4998	4407.260
$[90/0/90/F/90/0/90]_T$	23.481	1.5001	2727.870
$[90_4/F/90_4]_T$	17.450	1.4999	2569.550
$[0_4/F/0_4]_T$	55.129	1.5001	5472.640
$[90_4/F/0_4]_T$	40.406	1.4998	4338.280
$[90/0/90/0/F/0/90/0/90]_T$	22.563	1.5002	2963.470

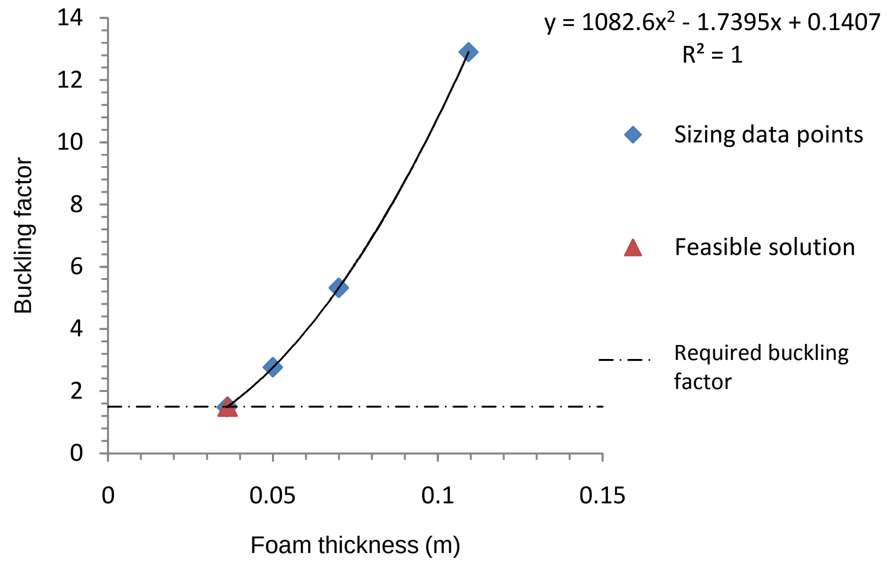

Figure 4.55 Buckling factor as a function of foam thickness for a composite sandwich layup $[90/F/90]_T$

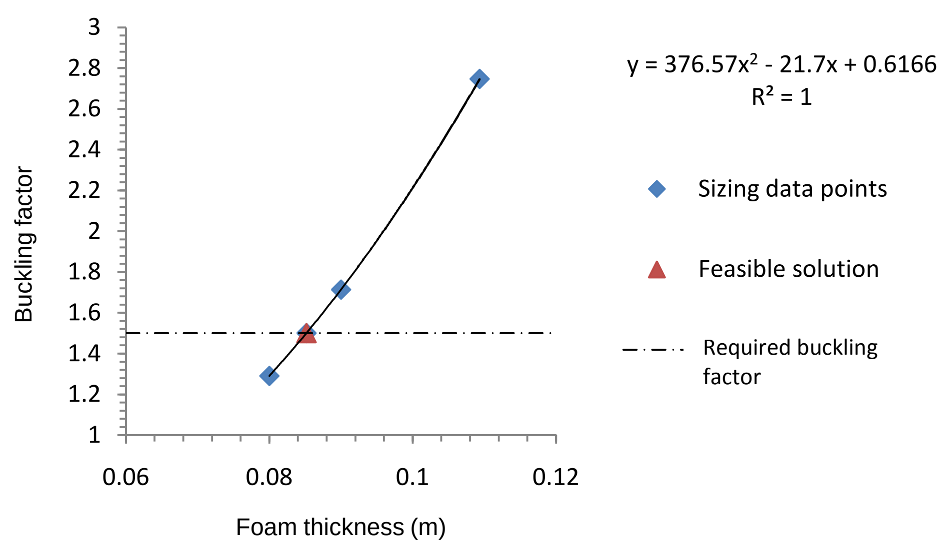

Figure 4.56 Buckling factor as a function of foam thickness for composite sandwich $[0/F/0]_T$

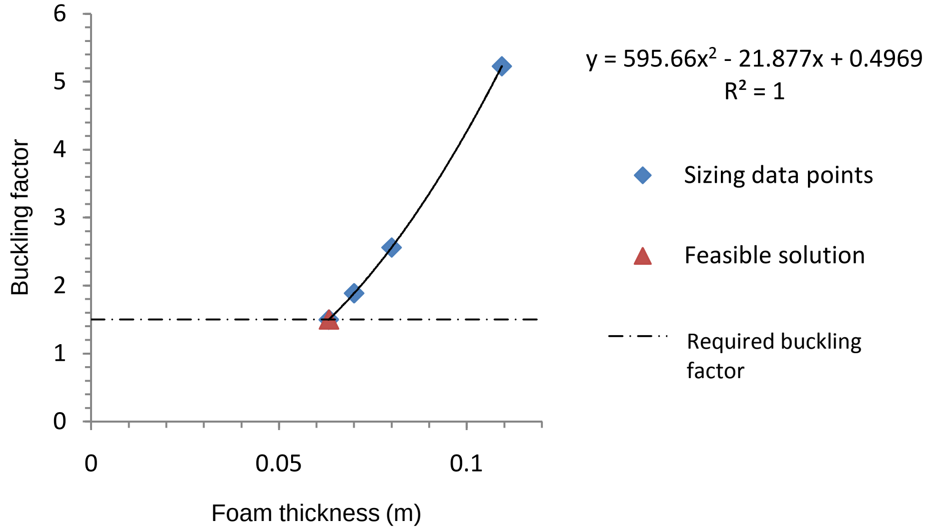

Figure 4.57 Buckling factor as a function of foam thickness for composite sandwich $[90/F/0]_T$

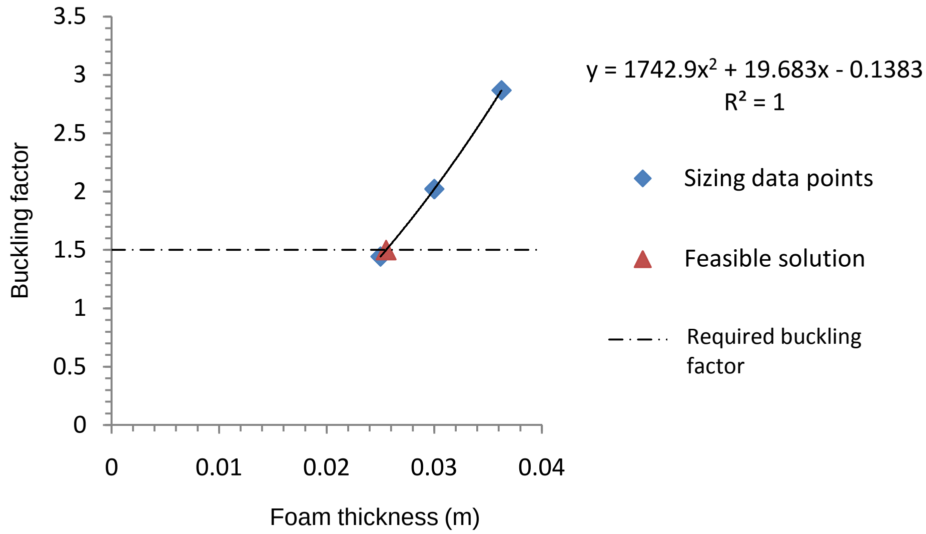

Figure 4.58 Buckling factor as a function of foam thickness for a composite sandwich composite of $[90_2/F/90_2]_T$

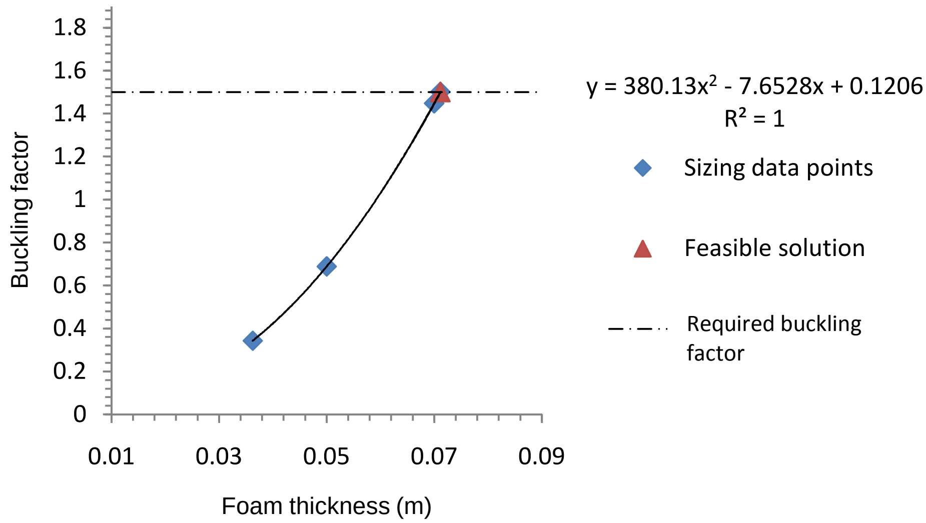

Figure 4.59 Buckling factor as a function of foam thickness for a composite sandwich layup of $[0_2/F/0_2]_T$

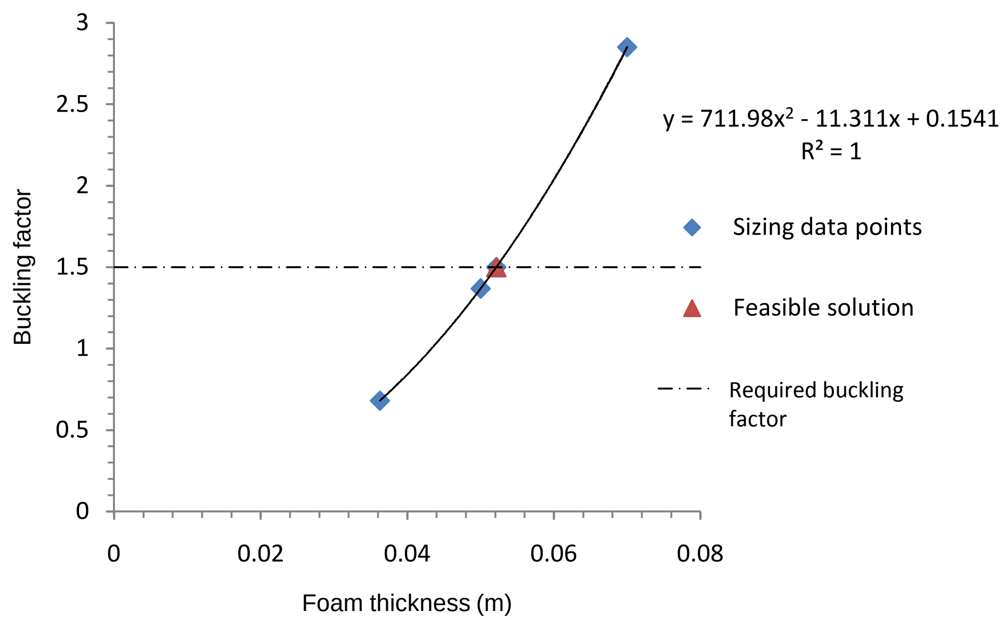

Figure 4.60 Buckling factor as a function of foam thickness for a composite sandwich layup of $[90_2/F/0_2]_T$

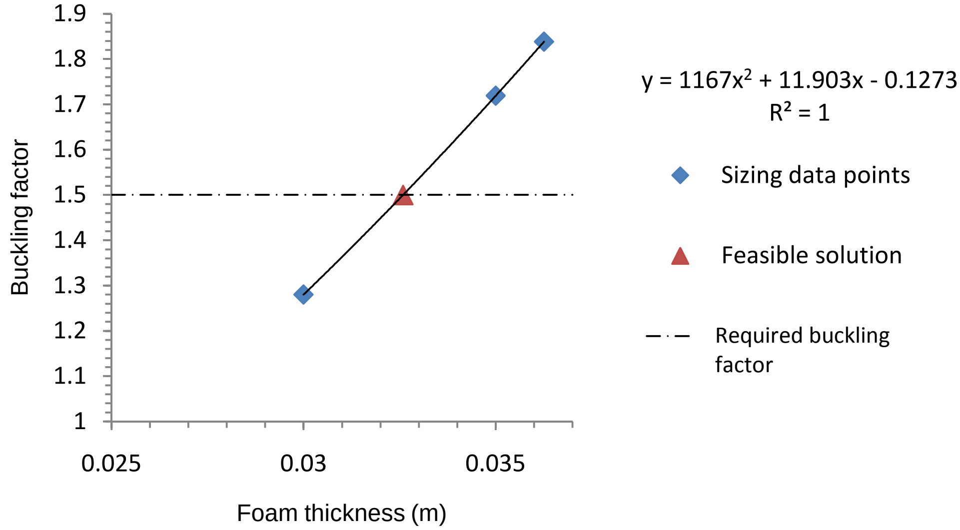

Figure 4.61 Buckling factor as a function of foam thickness for a composite sandwich layup of $[90/0/F/90/0]_T$

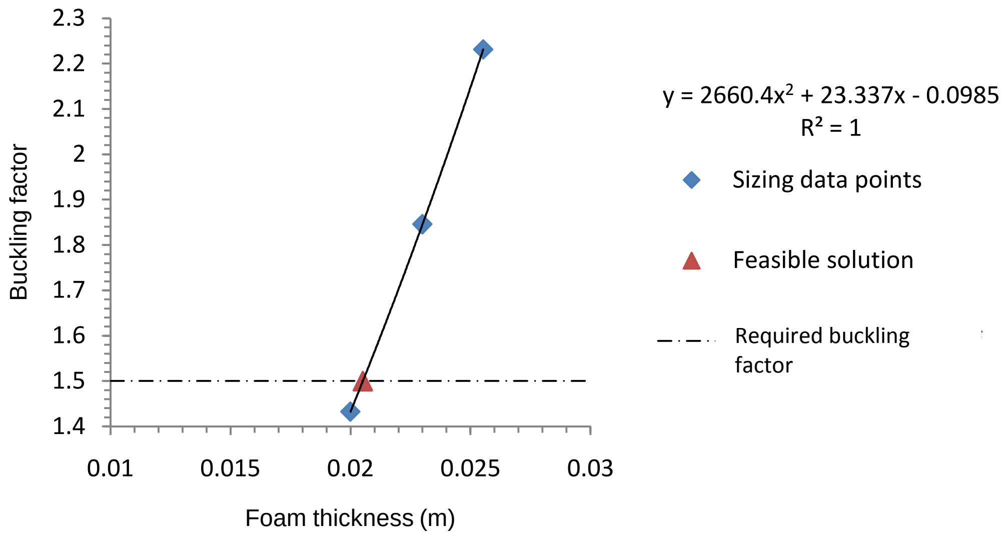

Figure 4.62 Buckling factor as a function of foam thickness for a composite sandwich layup of $[90_3/F/90_3]_T$

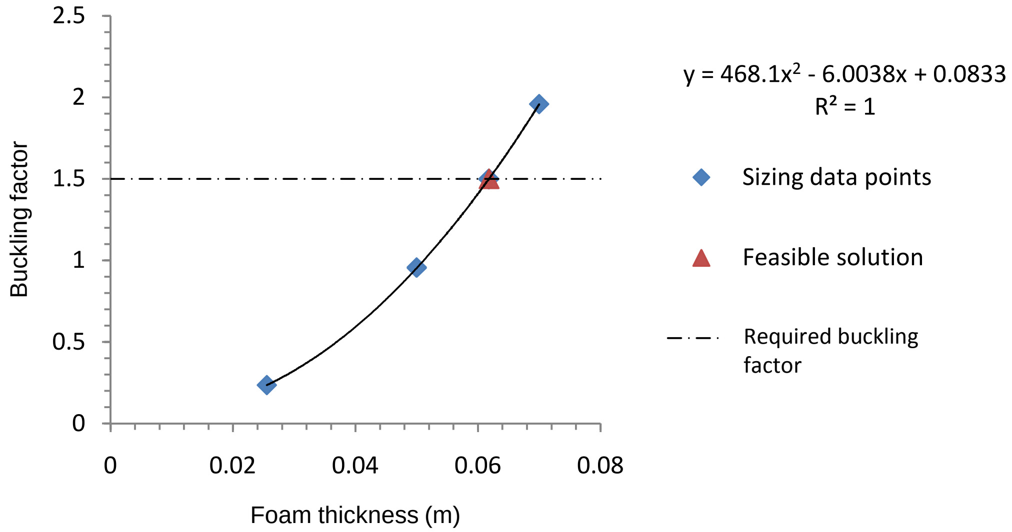

Figure 4.63 Buckling factor as a function of foam thickness for a composite sandwich layup of $[0_3/F/0_3]_T$

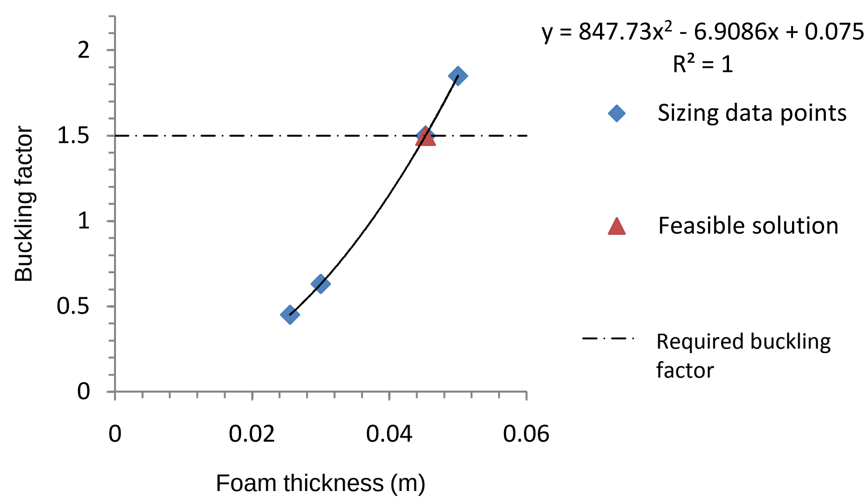

Figure 4.64 Buckling factor as a function of foam thickness for a composite sandwich layup of $[90_3/F/0_3]_T$

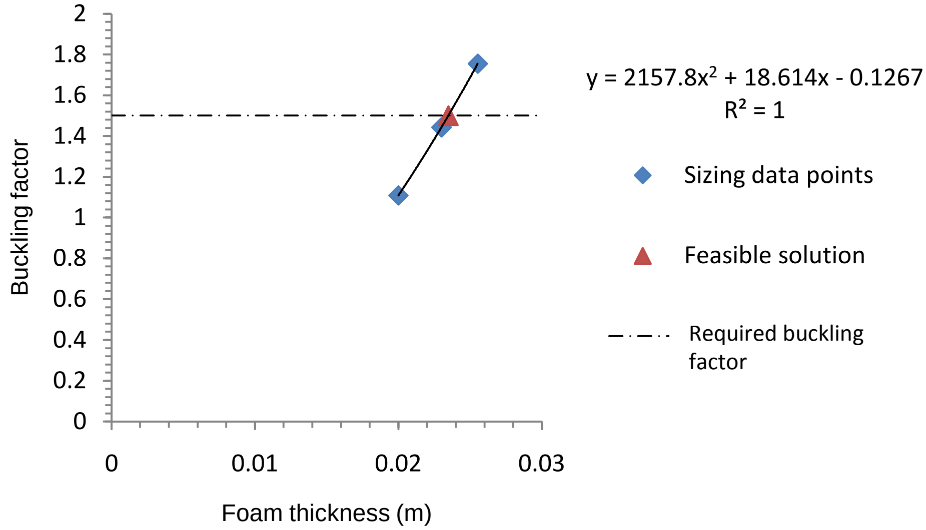

Figure 4.65 Buckling factor as a function of foam thickness for a composite sandwich layup of $[90/0/90/F/90/0/90]_T$

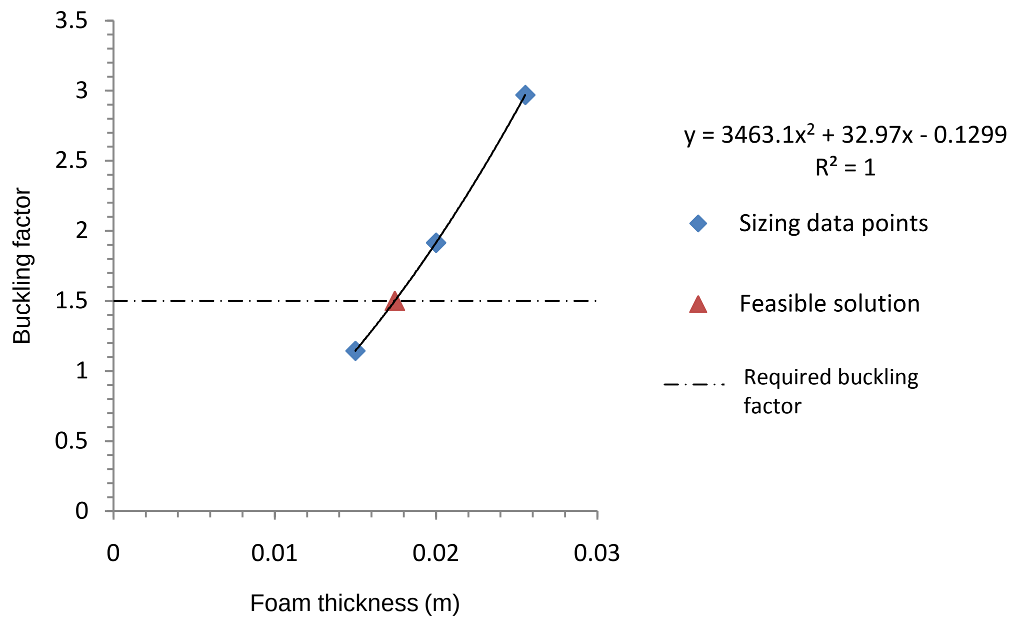

Figure 4.66 Buckling factor as a function of foam thickness for a composite sandwich layup of $[90_4/F/90_4]_T$

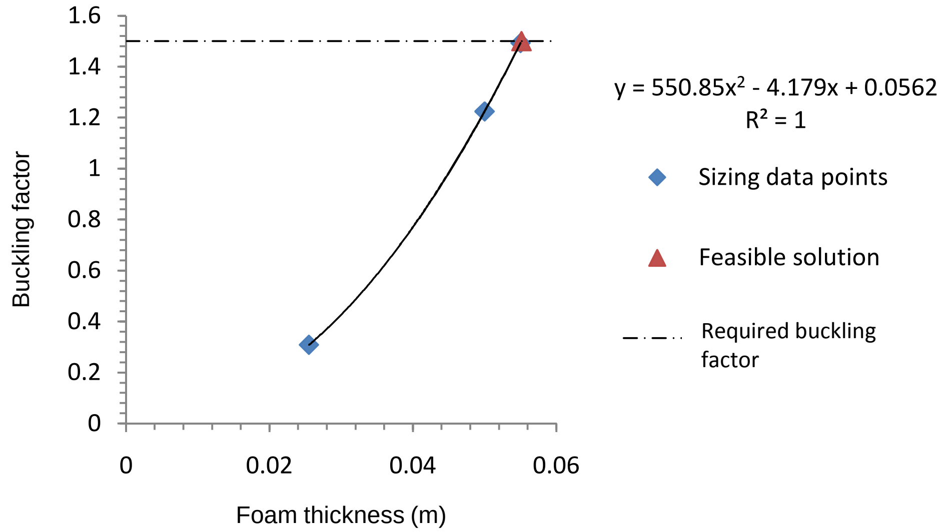

Figure 4.67 Buckling factor as a function of foam thickness for a composite sandwich layup of $[0_4/F/0_4]_T$

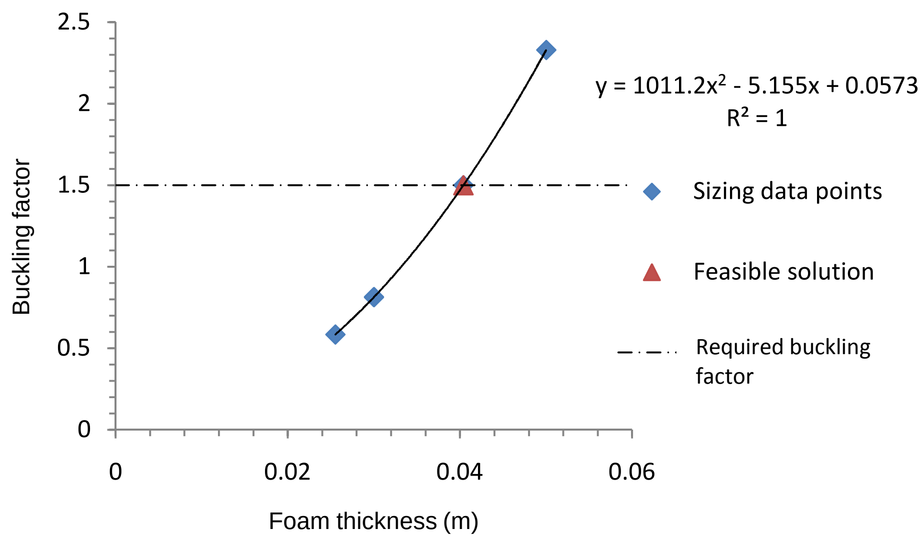

Figure 4.68 Buckling factor as a function of foam thickness for a composite sandwich layup of $[90_4/F/0_4]_T$

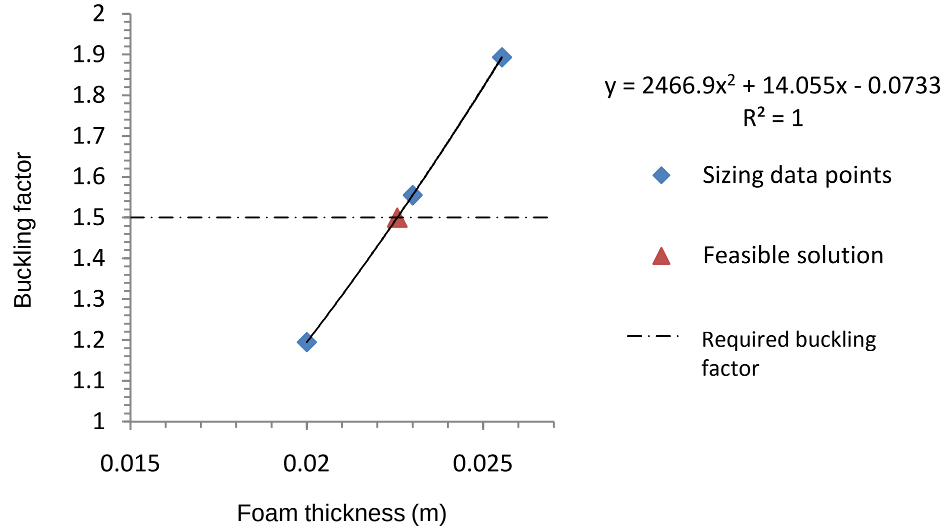

Figure 4.69 Buckling factor as a function of foam thickness for a composite sandwich layup of $[90/0/90/0/F/0/90/0/90]_T$

4.2.2.5 Optimization of Composite Sandwich Duct

After sizing for foam for each sandwich layup, an optimization study was conducted to find an optimum minimum weight solution from the feasible set of solutions obtained in the previous section. The feasible set of solutions are compared in Figure 4.70.

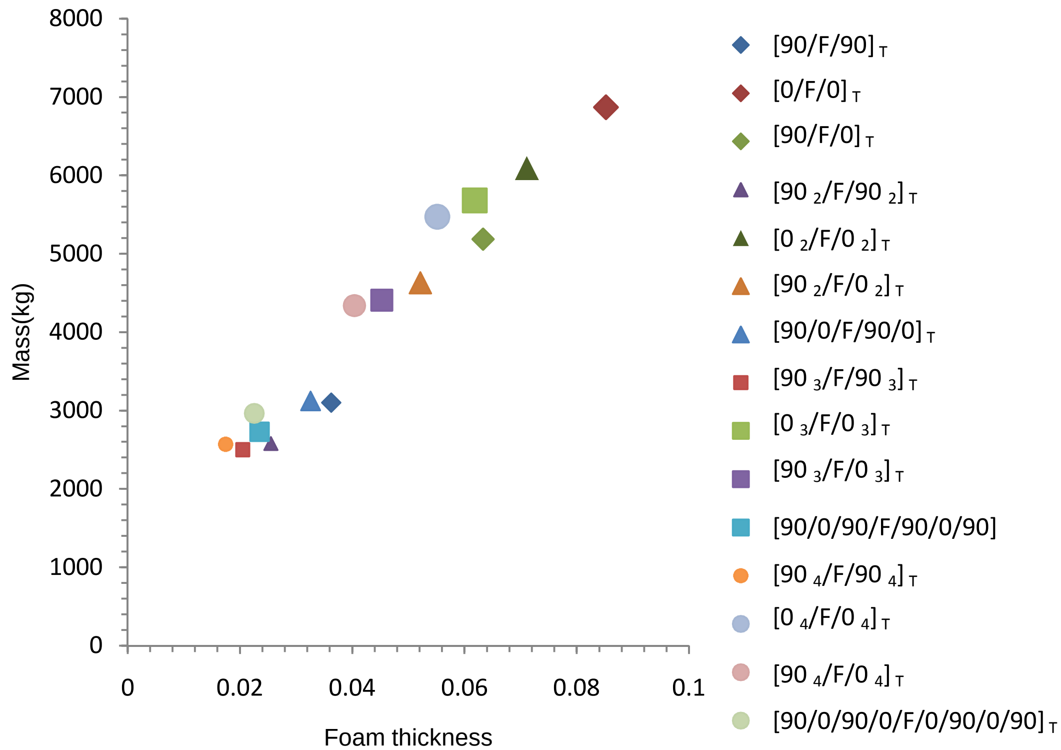

Figure 4.70 Optimization for minimum mass for composite sandwich duct

Based upon the results shown in Figure. 4.70, the optimum sandwich composite layup for the propulsive duct was $[90_3/F/90_3]_T$, t_f=20.515 mm for which the minimum duct mass was 2499.450 kg.

4.2.3 Structural Optimization of Duct of the Airship Operating at 65 kft

4.2.3.1 Sizing of Foam-Only Duct

The sizing of foam-only duct is performed first. The study showed that for the foam-only duct, the required foam thickness was 71.449 mm which resulted in buckling factor of 1.4999, and a corresponding duct mass of 5504.630 kg. The sizing procedure showing the determination of a quadratic function, for finding minimum foam thickness for duct at 65 kft above sea level is given in Figure 4.71.

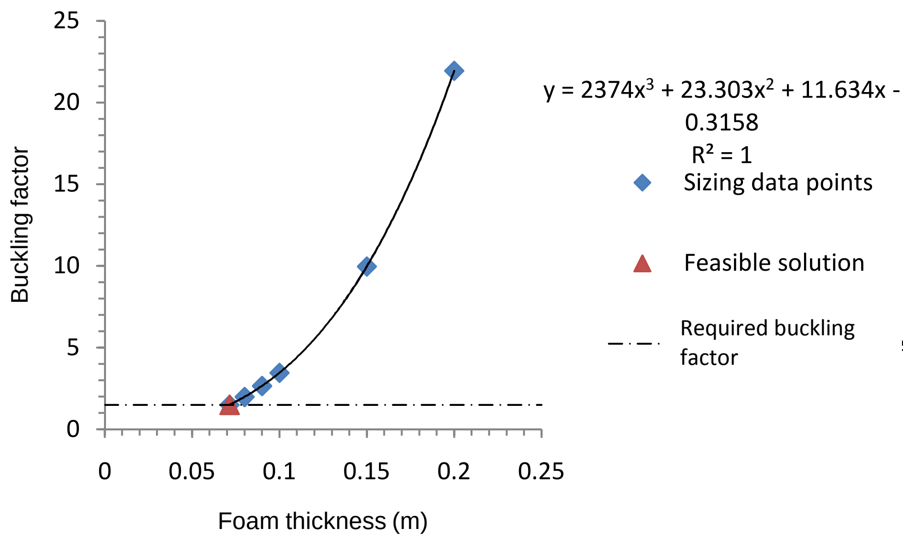

Figure 4.71 Buckling factor as a function of foam thickness for a foam-only duct.

4.2.3.2 Sizing of Graphite/Epoxy Laminate-Only Duct

The next step was to perform a sizing study of a composite duct made of graphite/epoxy composite laminate. The minimum number of plies required to prevent buckling, with their corresponding buckling factors and masses are presented in Table 4.12.

Table 4.12 Optimized graphite/epoxy laminate-only duct configurations at 65 kft

Fiber Orientation	Number of plies (n)	Buckling factor	Mass (kg)
$[90_n]_T$	45	1.5195	8422.220
$[0_n]_T$	103	1.5177	15772.500
$[(90/0)_n]_T$	27	1.4758	9890.910

The sizing procedure showing the determination of a quadratic function, for finding the minimum number of plies needed to satisfy the stability constraint for the layups $[90_n]_T$, $[0_n]_T$, and $[(90/0)_n]_T$ is given in Figures 4.72, 4.73, and 4.74, respectively.

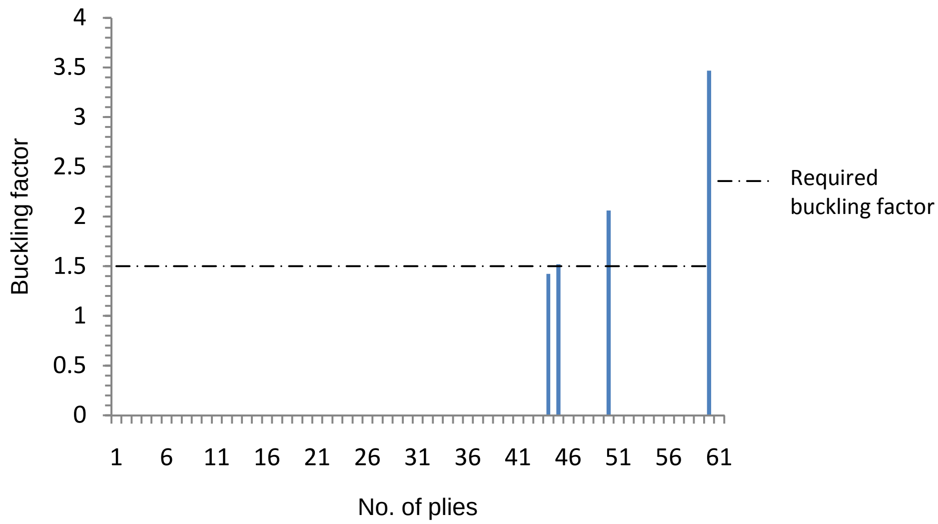

Figure 4.72 Buckling factor as a function of no. of plies for the layups $[90_n]_T$

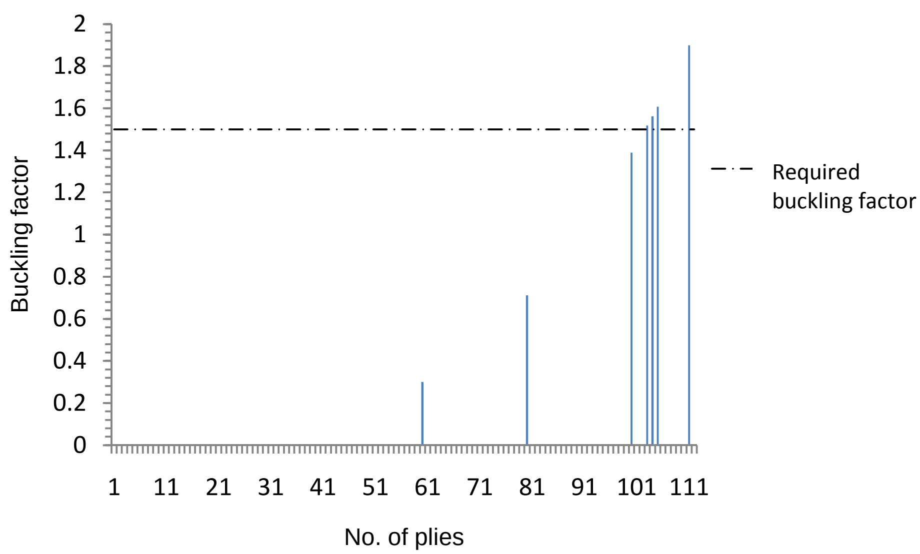

Figure 4.73 Buckling factor as a function of no. of plies for the layups $[0_n]_T$

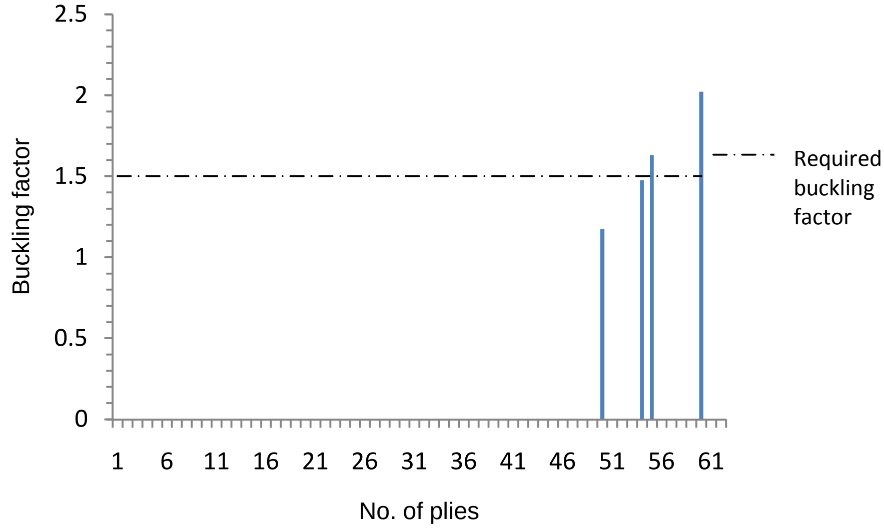

Figure 4.74 Buckling factor as a function of no. of plies for the layups $[(90/0)_n]_T$

4.2.3.3 Optimization of Graphite/Epoxy Laminate-Only Duct

After iterating for minimum number of plies for each layup, an optimization study was conducted to find an optimum minimum weight solution from the feasible set of solutions shown in Figure 4.75.

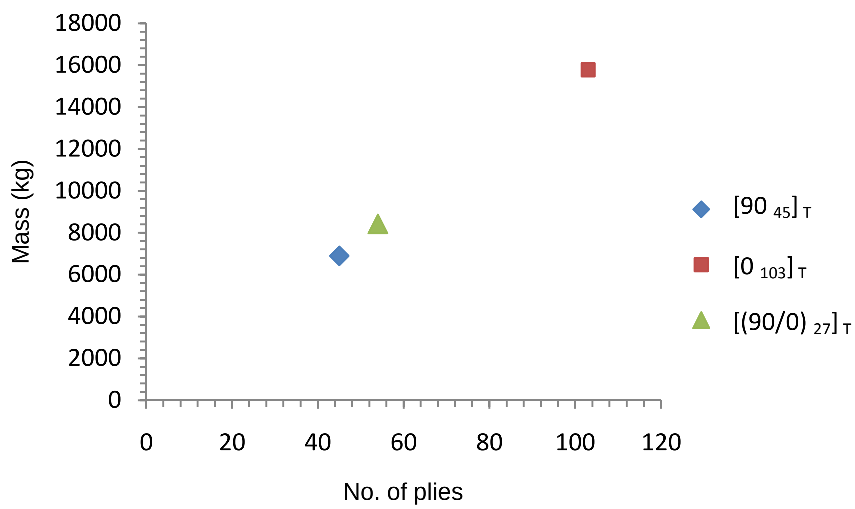

Figure 4.75 Optimization for minimum mass for graphite/epoxy laminate-only duct

Based upon the results shown in Figure. 4.75, the optimum composite layup for the propulsive duct was $[90_{45}]_T$ for which the minimum duct mass was 6890.910 kg.

4.2.3.4 Sizing of Composite Sandwich Duct

Sizing studies were conducted in ABAQUS for the sandwich layups as provided in Table 4.7. The number of plies in a face sheet was increased until the minimum mass of the latest configuration exceeded the minimum mass obtained in the previous configuration, whereupon the minimization process was ended. For this case, the mass of the two-ply sandwich layup was less than three-ply sandwich layup; henceforth the iteration process was ended. The sizing results for an airship operating at 65 kft above sea level are shown in Table 4.13.

Table 4.13. Optimized composite sandwich duct configurations for airship operating at 65 kft

Sandwich Layup	Foam thickness(mm)	Buckling factor	Mass (kg)
$[90/F/90]_T$	20.209	1.5005	1863.310
$[0/F/0]_T$	44.580	1.5000	3741.020
$[90/F/0]_T$	33.618	1.5002	2896.430
$[90_2/F/90_2]_T$	13.324	1.4995	1639.100
$[0_2/F/0_2]_T$	34.77	1.5000	3291.490
$[90_2/F/0_2]_T$	25.886	1.5004	2606.960
$[90/0/F/90/0]_T$	14.792	1.5000	1752.210
$[90_3/F/90_3]_T$	10.100	1.5004	1696.96
$[0_3/F/0_3]_T$	29.169	1.5002	3166.210
$[90_3/F/0_3]_T$	21.633	1.5003	2585.540
$[90/0/90/F/90/0/90]_T$	10.477	1.4998	1723.700

The sizing procedure showing the determination of a quadratic function, for finding minimum foam thickness for composite sandwich ducts for the layups provided in Table 4.7 are given in Figures 4.76 to 4.86.

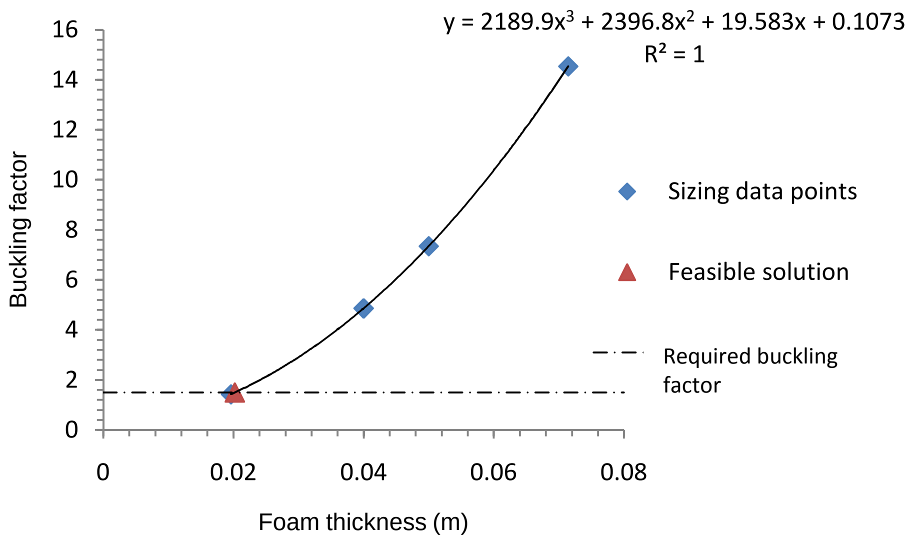

Figure 4.76 Buckling factor as a function of foam thickness for a composite sandwich layup [90/F/90] $_T$

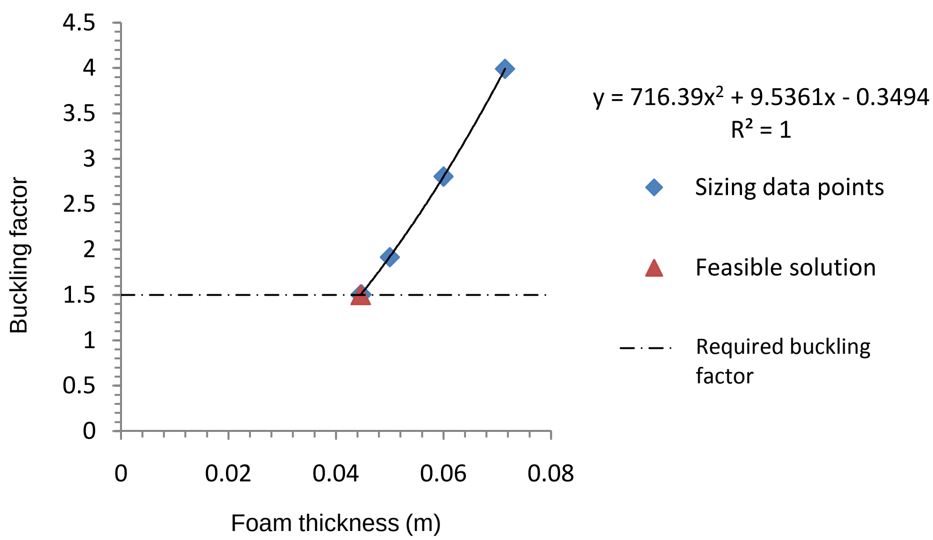

Figure 4.77 Buckling factor as a function of foam thickness for composite sandwich [0/F/0] $_T$

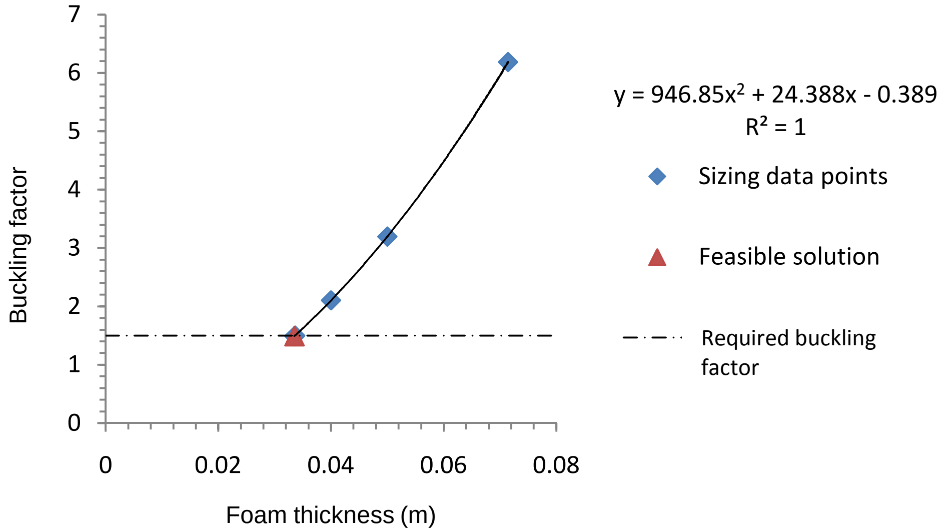

Figure 4.78 Buckling factor as a function of foam thickness for composite sandwich $[90/F/0]_T$

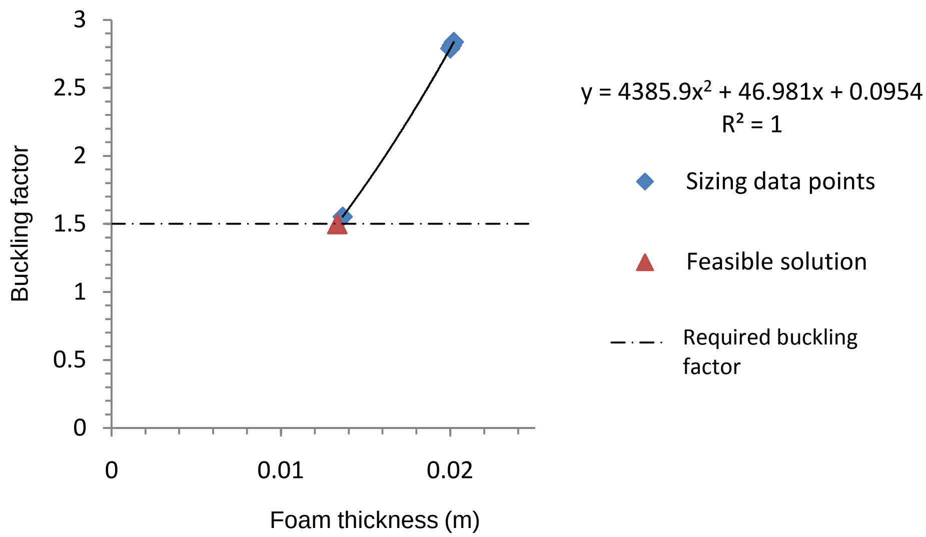

Figure 4.79 Buckling factor as a function of foam thickness for a composite sandwich composite of $[90_2/F/90_2]_T$

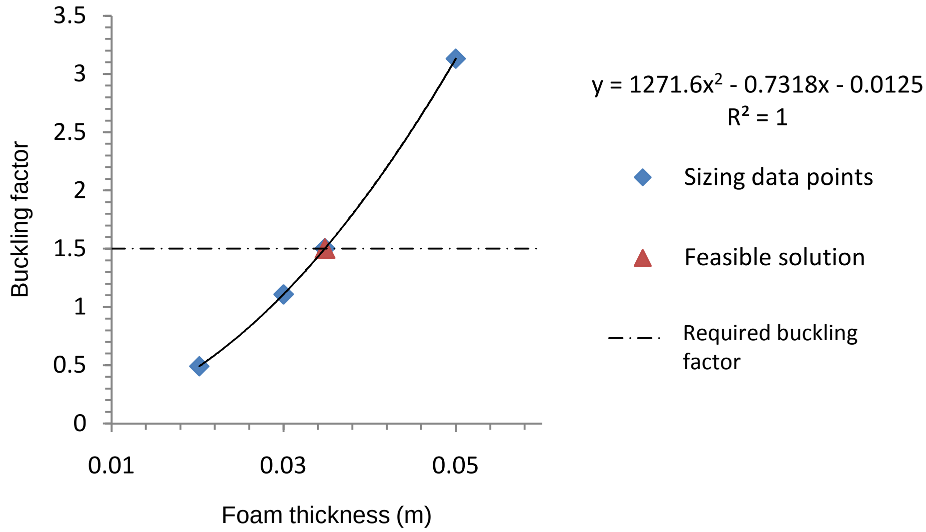

Figure 4.80 Buckling factor as a function of foam thickness for a composite sandwich layup of $[0_2/F/0_2]_T$

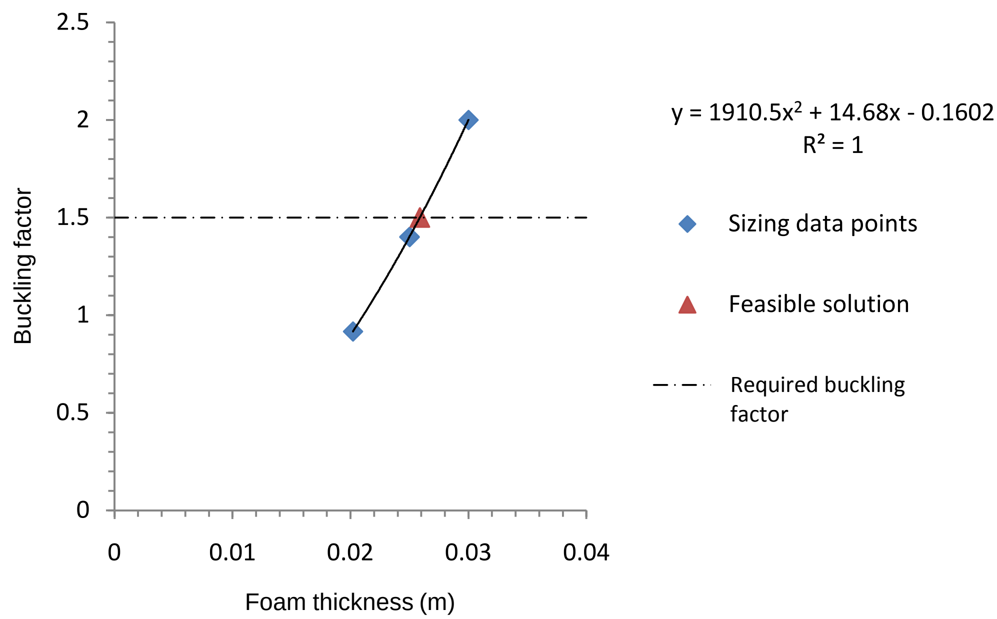

Figure 4.81 Buckling factor as a function of foam thickness for a composite sandwich layup of $[90_2/F/0_2]_T$

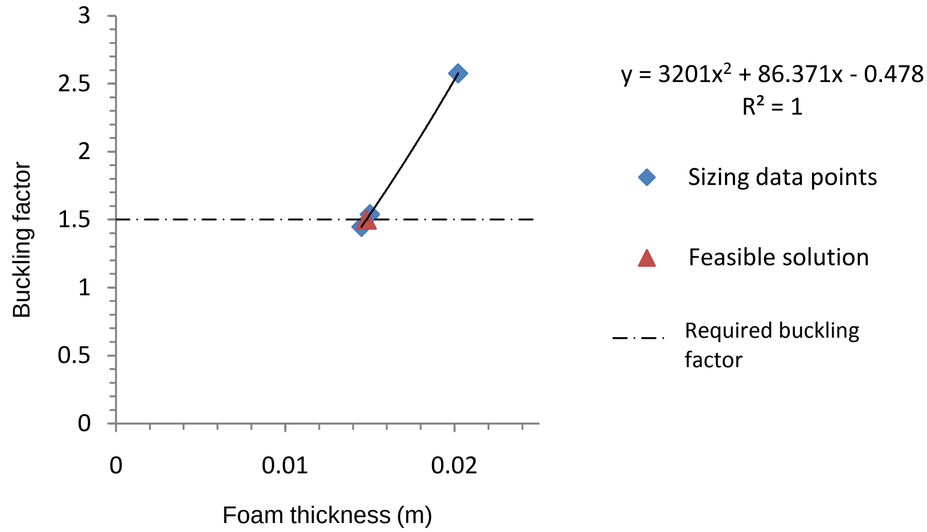

Figure 4.82 Buckling factor as a function of foam thickness for a composite sandwich layup of $[90/0/F/90/0]_T$

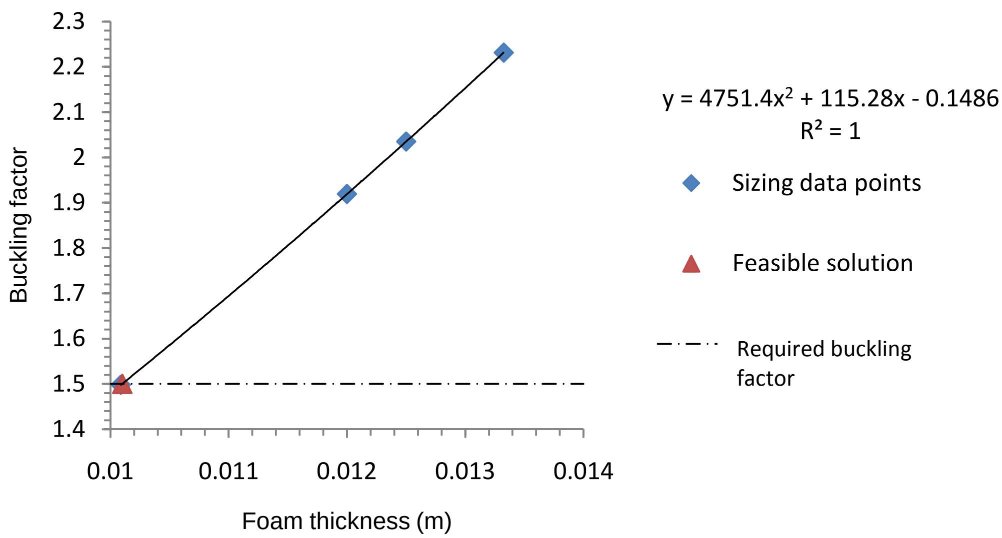

Figure 4.83 Buckling factor as a function of foam thickness for a composite sandwich layup of $[90_3/F/90_3]_T$

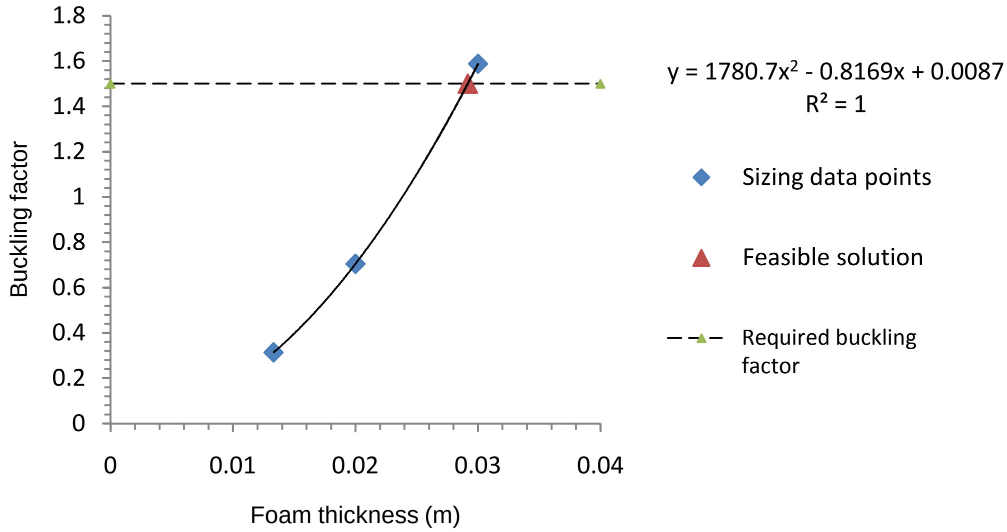

Figure 4.84 Buckling factor as a function of foam thickness for a composite sandwich layup of $[0_3/F/0_3]_T$

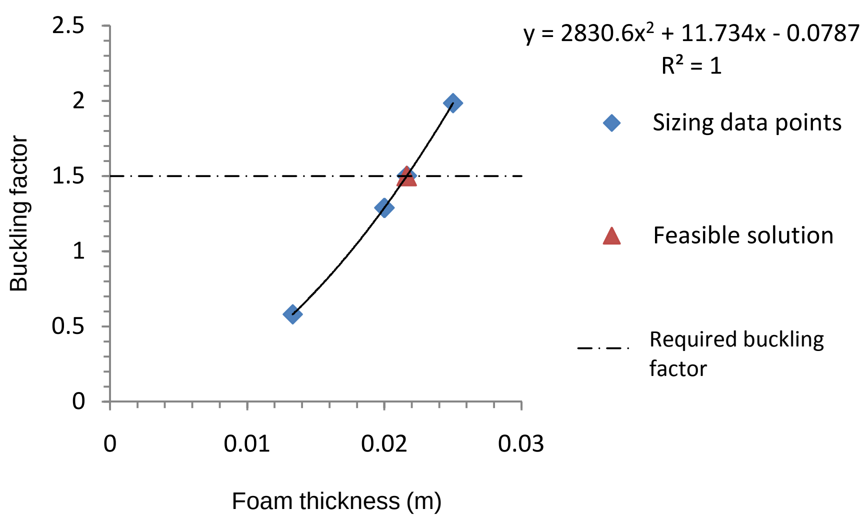

Figure 4.85 Buckling factor as a function of foam thickness for a composite sandwich layup of $[90_3/F/0_3]_T$

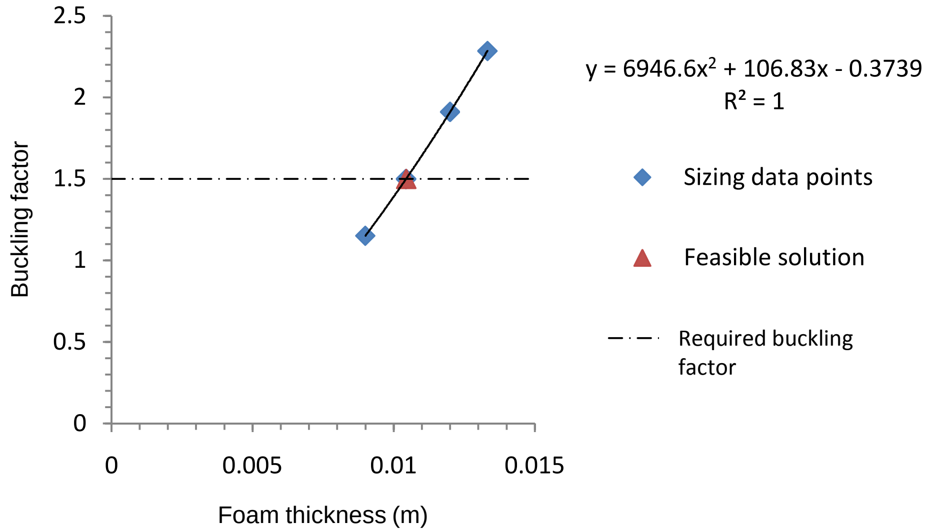

Figure 4.86 Buckling factor as a function of foam thickness for a composite sandwich layup of $[90/0/90/F/90/0/90]_T$

4.2.3.5 Optimization of Composite Sandwich Duct

After sizing for foam for each sandwich layup, an optimization study was conducted to find an optimum minimum weight solution from the feasible set of solutions shown in Figure 4.87. Based upon the results shown in Figure. 4.87, the optimum sandwich composite layup for the propulsive duct was $[90_2/F/90_2]_T$, t_f=13.324 mm for which the minimum duct mass was 1639.100 kg.

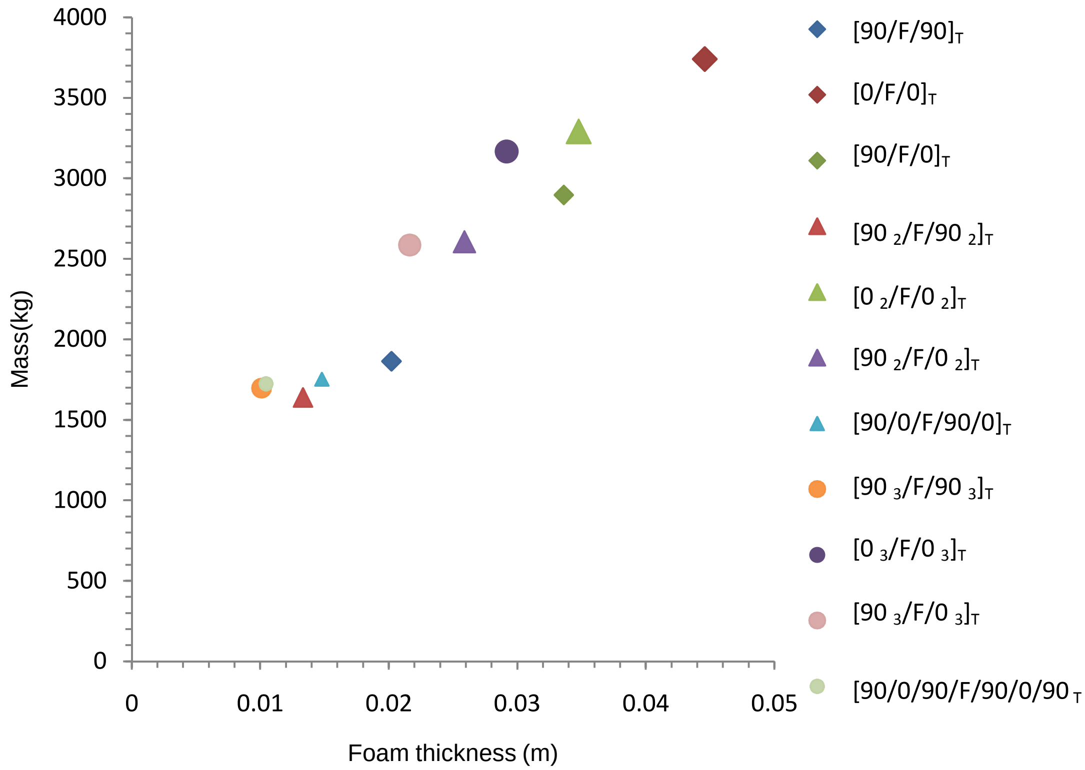

Figure 4.87 Optimization for minimum mass for composite sandwich duct

CHAPTER 5

RESULTS AND DISCUSSIONS

5.1 Minimum Weight Solution for Airship Operating at Sea Level

By comparing the optimized solutions of foam-only duct, graphite/epoxy laminate-only duct and sandwich duct, it was observed that the best possible minimum weight solution was given by sandwich composites. The Figure 5.1 demonstrates the significant weight reduction when composite sandwich were used for the airship operating at sea Level. The optimum sandwich for propulsive duct was found to be $[90_2/0/90_2]_T$, t_f=16.174 mm having the minimum duct mass of 1905.960 kg. The mass of the duct reduced to 70% as compared to mass of foam-only duct, and it reduced to 79%, compared to optimized graphite/epoxy laminate-only duct. The study also revealed that the optimum orientation of ply for sandwich will be 90˚ i.e. fiber in the hoops stress direction.

5.2 Minimum Weight Solution for airship working at altitude of 32.5 kft

For the airship stationed at 32.5 kft, the optimum sandwich for the propulsive duct was $[90_3/F/90_3]_T$, t_f=20.515 mm for which the minimum duct mass was 2499.450 kg. Similarly, the optimized solution for sandwich composite duct yielded significant weight reduction for the same stability constraint compared to foam-only duct and graphite/epoxy laminate-only duct. The mass of the duct reduced to 70% as compared to mass of foam-only duct, and it reduced to 78%, compared to optimized graphite/epoxy laminate-only duct. The optimized ply orientation of composite sandwich for the graphite/epoxy was 90˚.

5.3 Minimum Weight Solution for airship working at altitude of 65 kft

For the airship stationed at 65 kft, the optimum sandwich for the propulsive duct was $[90_2/F/90_2]_T$, t_f=13.324 mm for which the minimum duct mass was 1639.10 kg. The optimized solution for sandwich composite duct yielded significant weight reduction for the similar stability constraint compared to foam-only duct and graphite/epoxy laminate-only duct. The mass of the duct reduced to 70% as compared to mass of foam-only duct, and it reduced to 76% for optimized graphite/epoxy laminate-only duct. As explained above for all the cases above, the optimized ply orientation of composite sandwich for the graphite/epoxy was 90˚.

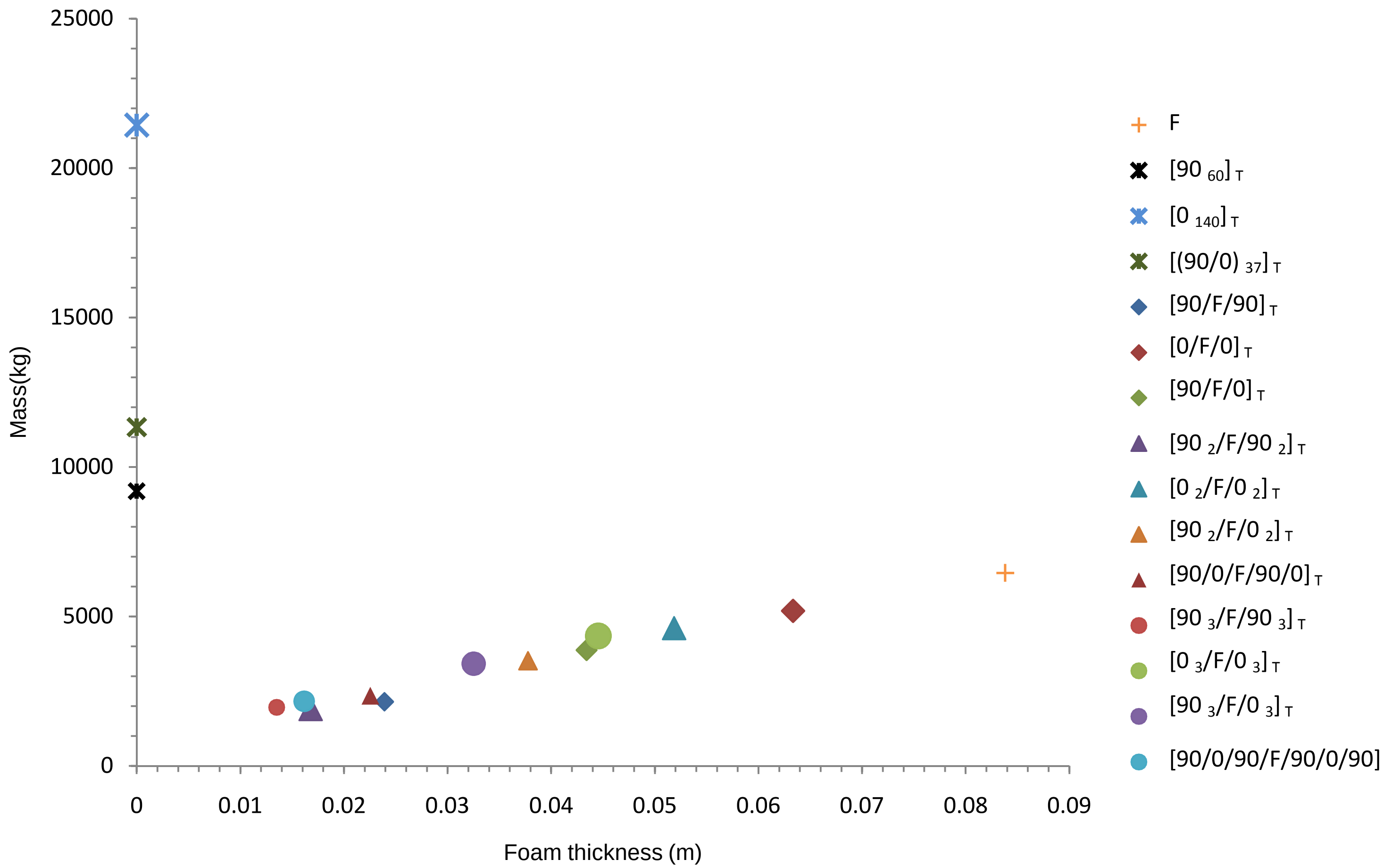

Figure 5.1 Mass as a function of foam thickness for at sea level

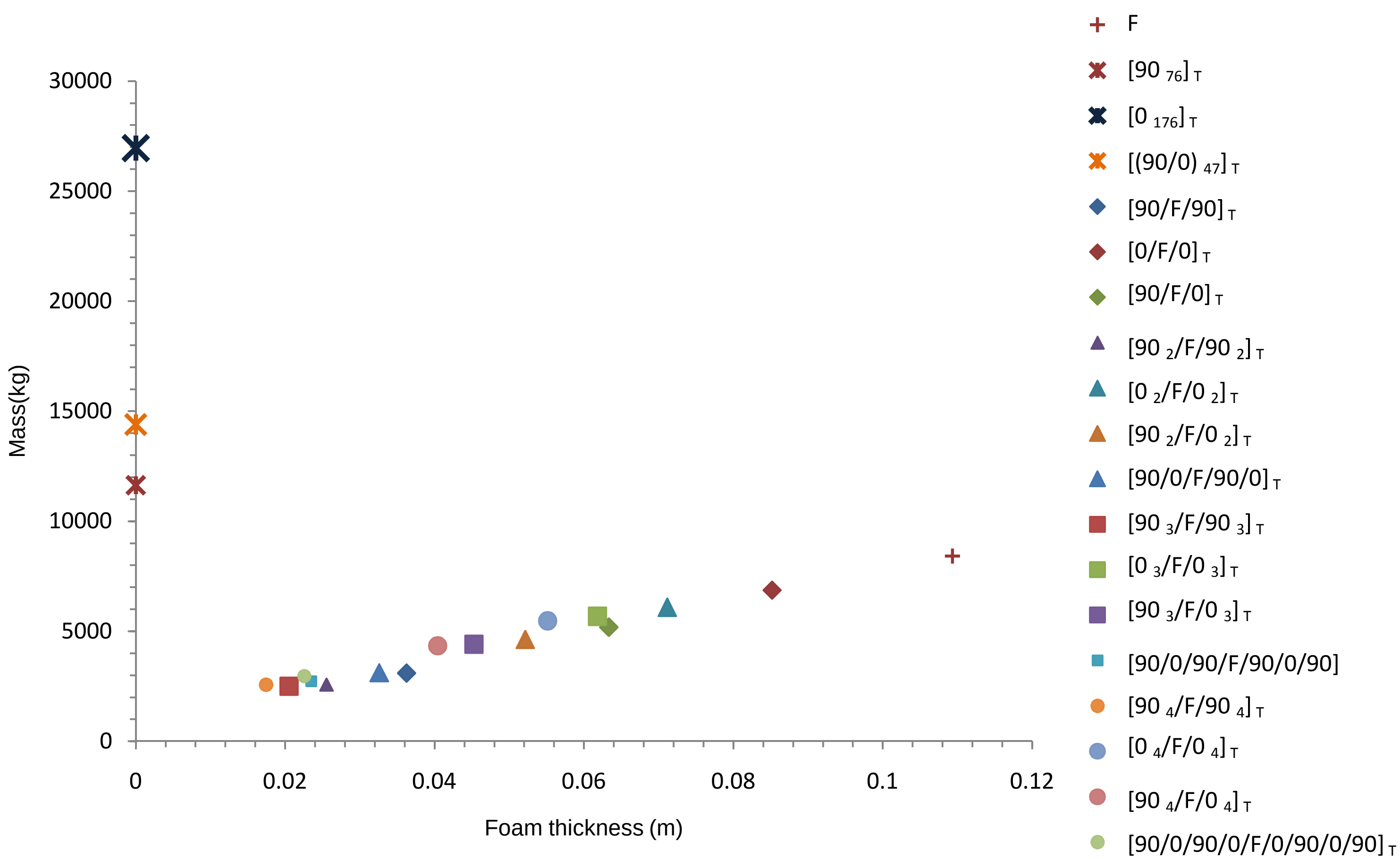

Figure 5.2 Mass as a function of foam thickness for 32.5 kft

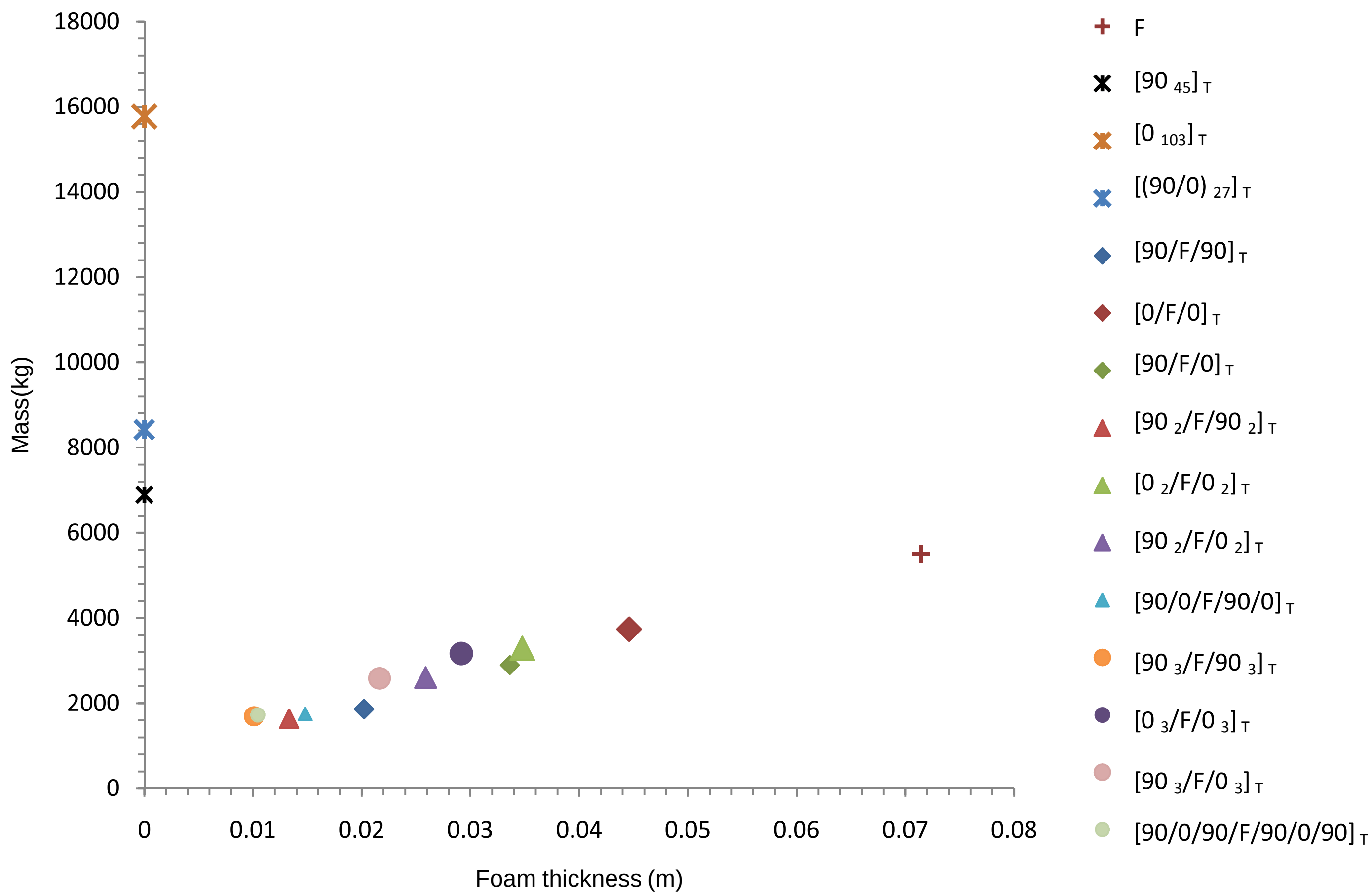

Figure 5.3 Mass as a function of foam thickness for 65 kft

CHAPTER 6

CONCLUSIONS AND RECOMMENDATIONS

6.1 FEM-Based Minimum Weight Structural Optimization Methodology under Stability Constraints

In this work a weight-minimization investigation for composite sandwich duct in a toroidal airship subjected to stability constraints under applied lateral pressure was undertaken using a commercially available FEM code, ABAQUS v6.10. The structural optimization methodology involved sizing of a foam-only duct, a graphite/epoxy laminate-only duct, and a composite sandwich duct having graphite/epoxy face sheets and foam core for the airship operating at sea level, 32.5 kft, and 65 kft above sea level. The results from these optimization studies show that the best possible minimum weight solution was given by a composite sandwich configuration. The study revealed that the optimum ply orientation will be always 90˚, which follows when considering that the fibers are running in the same direction as the hoop stresses. The optimization methodology developed in the present research can be generalized in identifying minimum weight duct configurations for a number of representative combinations of duct geometry, material properties, applied pressure loading and generic operating levels.

6.2 Recommendations

1. In the study the buckling of perfectly circular cylinders was only considered. A linear analysis of the problem considering geometric imperfections should be conducted to investigate the sensitivity of buckling load to imperfections.
2. To further verify the accuracy of the FEM solutions an experimental investigation could be conducted. However the experimental setup of such a problem is difficult to achieve due to complex loading condition.

3. The optimized fiber orientation angle is 90°. But in practice it is not advisable to put layers of the same orientation together due to chances of failure caused by splitting of fibers by loading across the fibers. Therefore, the inclusion of0° layers should be considered.

REFERENCES

[1] Crouch, T. D., “Lighter Than Air,” The John Hopkins University Press, Baltimore, 2009, Chapters 1, 2.

[2] Suryanarayana, G. K., Pauer., H, and Meier, G. E. A, “Bluff-Body Drag Reduction by Passive Ventilation,” *Experiments in Fluid,* 16, pp 73-81, 1993.

[3] Batdorf, S.B., “A Simplified Method of Elastic-Stability Analysis for Thin Cylindrical Shells,” *NACA Report 874*, 1947.

[4] Hao, B., Cho, C. and Lee, S.W.,” Buckling and Postbuckling of Soft-core Sandwich Plates with Composite Facesheets,” SpringerLink, *Computational Mechanics* 25, pp 421-429, 2000.

[5] Adali, A., Richter, A. Verijenko, V.E. and Summers, E.B., “Optimal Design of Hybrid Laminates with Discrete Ply Angles for Maximum Buckling Load and Minimum Cost,” Elsevier Science Limited, *Composite Structures,* 32, pp 409-415, 1995.

[6] Walker, M. and Smith, R.,” A Procedure to Select the Best Material Combinations and Optimally Design Composite Sandwich Cylindrical Shells for Minimum Mass,” Elsevier Science Limited, *Material and Design* 27, pp 160-165, 2006.

[7] Walker, M., Reiss, T. and Adali, S., “Minimum Weight of Composite Hybrid Shells via Symbolic Computations, ” Elsevier Science Limited, *J Franklin Institute* Vol. 334B, No. 1, pp 47-56, 1997.

[8] Xie, Y.J., Yan H.G., and Liu Z. M., “Buckling Optimization of Hybrid-Fiber Multilayer-Sandwich Cylindrical Shells under External Lateral Pressure,” Elsevier Science Limited, *Composite Science and Technology* 56, pp 1349-1353, 1997.

[9] Liang, C.C. and Chen, H.W.," Optimum Design of Fiber-Reinforced Composite Cylindrical Skirts for Solid Rockets Cases Subjected to Buckling and Overstressing Constraints," Elsevier Science Limited, *Composites*, Part B 34, pp 273-284, 2003.

[10] ABAQUS v6.10 Reference Manual.

[11] Hyer, M.W., "Stress Analysis of Fiber-Reinforced Composite Materials," WCB McGraw-Hill, New York, 1998, Chapter 2, pp 58.

[12] Daniel, I. M., Gdoutos, E.E. and Rajapakse, Y.," Major Accomplishment in Composite Material and Sandwich Structures," Springer, New York, 2010, Part IV, pp 647.

[13] Leishman, J.G.," Principles of helicopter aerodynamics," Cambridge University Press, New York, 2006.

BIOGRAPHICAL INFORMATION

Urmi B. Khode was born on March 16th, 1986 in Ujjain, India. In August 2008 she graduated with a Bachelor's of Science in Mechanical Engineering from Raipur Institute of Technology, Raipur, India. Due to her interest in aerospace structures, she joined the graduate program at The University of Texas at Arlington to study for a Masters in Aerospace Engineering in January 2009. She is currently a Graduate Research Assistant in Wind Energy Research Laboratory/Tailored Composites & Smart Structures Laboratory at UT Arlington.